

---

**MSc Thesis**

---

**Experimental study on dynamic failure  
characteristics of confined coal under cyclic  
impact load**

---

**Author: Chunyang Dong**

**Supervisor: Professor Beijing Xie**

Date(18/05/2021)



---

School of Emergency Management and Safety Engineering  
China University of Mining and Technology (Beijing)

Beijing Haidian district Xueyuan Rd,Ding 11.  
Yifu Building 1118





---

## **Declaration of Authorship**

---

„I declare in lieu of oath that this thesis is entirely my own work except where otherwise indicated. The presence of quoted or paraphrased material has been clearly signaled and all sources have been referred. The thesis has not been submitted for a degree at any other institution and has not been published yet.”



---

## Abstract

---

In this paper, the combination of experimental, theoretical analysis and data analysis methods is used. Applying Hopkinson experimental platform of triaxial confining pressure, the selected 22 samples were tested 60 times. The mechanism of underground cumulative damage rock burst is simulated, and the dynamic failure characteristics of confined coal under cyclic impact load are studied. The SHPB system of triaxial confining pressure was used to test the coal samples with or without confining pressure, different damage impact times, and different damage impact velocities. The change characteristics of elastic modulus, stress-strain, strain rate, and damage degree are analyzed to study the damage evolution law and dynamic mechanical properties of coal. The main conclusions are: (1) When the specimen is subjected to cyclic impact under triaxial confining pressure, it will go through the compaction stage in the early stage to increase the bearing capacity of the specimen. When the damaging impact reaches a certain number of times, the compaction speed of the specimen is lower than the crack development speed, and the specimen begins to produce damage. (2) After 4 times of 0.2MPa low strength impact, the cumulative damage of samples is negative, -5.77%, -7.11%, -10.01% and -13.95% respectively. (3) Under triaxial confining pressure, the coal has a significant strain rate effect. The higher the impact velocity is, the higher the stress peak value, and the corresponding strain rate peak value can be achieved. (4) Under the condition of triaxial confining pressure, with the increase of failure impact velocity, the greater the stress peak value of the specimen, the more serious the damage or breakage. Through the research of this paper, it provides experimental basis and reference for further understanding the failure mechanism of coal under dynamic load, the failure mechanism of rock burst and the evaluation of long-term stability of rock engineering.

**Keywords:** cyclic impact load, damage evolution of coal, triaxial confining pressure SHPB, different impact velocity, dynamic mechanical properties



---

# Table of Contents

---

Declaration of Authorship .....	I
Abstract .....	III
Table of Contents .....	V
1 Introduction.....	1
1.1 Background and significance of this research .....	1
1.2 Research status .....	3
1.2.1 Current Status of Research on Impact Failure of Coal and Rock under Dynamic Load .....	3
1.2.2 Research status of cyclic damage evolution and dynamic load failure of coal and rock materials .....	6
1.3 Research contents and methods .....	8
1.3.1 Main research contents .....	8
1.3.2 Research methods and technical route .....	9
2 Dynamic impact failure system and experiment of confined coal under cyclic impact load .....	11
2.1 Introduction.....	11
2.2 Impact failure system of triaxial confining pressure dynamic load.....	11
2.3 dynamic impact failure experiment of coal under triaxial confining pressure under cyclic impact load .....	17
2.3.1 SHPB experimental principle.....	17
2.3.2 Preparation and testing of specimens .....	19
2.3.3 Experimental steps .....	24
2.4 Experimental results of dynamic impact damage of triaxial pressure coal with cyclic impact loading.....	27
2.4.1 Uniaxial compression specimen crushing results.....	27
2.4.2 Triaxial pressure specimen crushing results .....	31
2.5 High-frequency noise reduction processing of the signal .....	35
2.6 Summary of the chapter .....	36
3 Analysis of dynamic impact damage evolution characteristics of pressurized coal under cyclic impact loading .....	38
3.1 Introduction.....	38
3.2 Selection of damage variable .....	39
3.3 Study of damage evolution characteristics of coal .....	43
3.3.1 Specimen damage evolution stress-strain curve analysis.....	43
3.3.2 The relationship between the peak stress and damage impact times.....	48



3.3.3 Relationship between the average strain rate and the number of damage impacts .....	49
3.3.4 Triaxial Surrounding Pressure Damage Evolution Law of Coal.....	52
3.4 Summary of the chapter .....	56
4 Analysis of dynamic impact failure characteristics of triaxial confining coal .....	58
4.1 Introduction.....	58
4.2 Mechanical properties analysis of dynamic load impact damage of damaged coal under triaxial pressure conditions .....	58
4.3 Dynamic mechanical characterization of coal with different impact velocities under triaxial pressure .....	63
4.3.1 Analysis of the stress-strain curve of coal at different impact velocities .....	63
4.3.2 Time course analysis of strain rate curve of coal under different impact velocities.....	65
4.4 Energy dissipation analysis of coal with different impact velocities under triaxial pressure.....	67
4.5 Summary of the chapter .....	71
6 Conclusions and outlooks.....	73
6.1 Conclusions .....	73
6.2 Outlooks .....	74
Reference .....	76

# 1 Introduction

---

## 1.1 Background and significance of this research

---

With the expansion of the construction scale and the increase of the demand for resources, the available space and resources on the surface and shallow layer of the surface are decreasing year by year, and many rock mass projects continue to go deep. The mining depth of various mineral resources has reached kilometer level [1-6]. After deep space development and resource mining construction, the original mechanical balance around the damaged coal and rock mass is broken, and the stress field changes. The influence of stress change on coal and rock mass is accompanied by the problem of rock mechanics, such as rock burst, stope pressure fluctuation, roadway instability, coal and gas outburst and other coal rock dynamic damage phenomena. These mine mechanics problems not only affect the safe and efficient mining of mineral resources, but also damage the natural environment to a certain extent. This has also become a hot topic of many scholars [7-10].

In recent years, disasters and accidents have occurred frequently in China due to the phenomenon of rock bursts [11-13]. On February 22, 2020, a rock burst accident occurred in the Longkun Mine of Shandong Xinjulong Company, which caused 4 people to be trapped underground. On June 9, 2019, a rock burst accident occurred in the transportation roadway of the 305 fully-mechanized mining face of Jimei Longjiabao Coal Mine, resulting in 12 injuries, 9 deaths, and a direct economic loss of 19.06 million yuan. On October 20, 2018, a major rock pressure accident occurred in the spillway and connecting lane at the working face of Shandong Longyun Coal Industry, resulting in 21 deaths. On November 11, 2017, a major rock burst accident occurred in the transportation roadway of the 702 fully-mechanized mining face of Hongyang No. 3 Mine in Shenyang, Liaoning, resulting in 10 deaths. Because rock bursts are sporadic, complex, and destructive, they often cause casualties, waste of resources, and property losses, and seriously affect the development of the national economy [14-17].

The mechanical properties of coal materials under dynamic loads are the basic parameters for studying the mechanism of coal dynamic damage disasters. The dynamic mechanical properties of coal and rock masses have attracted many

researchers in recent years <sup>[18,19]</sup>. In various underground projects, it is difficult to conduct field experiments with the actual size of coal and rock masses. Therefore, it is a research hotspot in rock mechanics, engineering mechanics and materials science to reflect the properties of materials in actual engineering through small-scale model tests. After more than 70 years of development, the separated Hopkinson bar has become a basic method for studying the dynamic mechanical properties of materials <sup>[20-22]</sup>.

Previous work has mostly used uniaxial Hopkinson rods to conduct physical experiments or numerical simulations on the dynamic mechanical properties of coal rock masses or the breakage characteristics of coal rock masses by a single strike of triaxial pressure. The response of materials under dynamic impact loads in uniaxial tension, compression or triaxial fixed circumferential pressure is used to analyze the propagation law of stress waves and thus determine the dynamic performance parameters and dynamic mechanical characteristics of coal rock masses. It is neglected that in the occurrence of coal-rock dynamic disaster, the breakage of coal body may be due to the multiple changes of stress field around the coal body during the mining process, and the impact energy of different sizes impact it several times, so that it accumulates the crushing energy and cracks expand, which eventually leads to the breakage, such as the impact ground pressure in the form of cumulative damage. The study and simulation of dynamic mechanical properties and rock dynamics disaster dynamics processes of coal rock bodies using only uniaxial tension, compression or triaxial perimeter pressure single strikes are seriously inadequate <sup>[23-28]</sup>. Therefore, in this paper, a triaxial enclosing pressure dynamic load separated Hopkinson bar (SHPB) impact damage test platform is used to conduct a combination of crushing impact experiments on coal bodies with and without enclosing pressure conditions, different impact times, and different impact velocities to analyze the dynamic load impact damage characteristics of coal bodies and determine the triaxial pressure dynamic mechanical properties of coal samples under different damage times and impact velocities. It provides experimental basis and reference for the study of coal body damage evolution law, dynamic mechanical properties, damage mechanism of impact ground pressure in the form of cumulative damage, and coal-rock dynamic disaster prevention and warning.

## 1.2 Research status

---

### 1.2.1 Current Status of Research on Impact Failure of Coal and Rock under Dynamic Load

---

The research of blasting impact and in-situ stress disturbance in the process of tunnel excavation and mining involves the dynamic mechanical properties of coal and rock materials. The mechanism of coal rock dynamic disaster and rock burst is also related to the dynamic mechanical properties of coal rock materials. There are great differences between the mechanical properties of coal and rock materials under static load and dynamic load. Scholars have also carried out a series of experimental research on this research direction.

Zhai Yue et al <sup>[30]</sup> conducted uniaxial impact damage tests on granite and concrete specimens with different strain rates using a modified separated SHPB compression bar, and showed that the strain rate had an effect on the strength of the rock material, the form of material fragmentation, and the degree of fragmentation, but had little effect on the damage strain, elastic modulus, and energy absorption rate of the material.

FREW D J et al <sup>[31]</sup> used a modified detached Hopkinson rod to impact rock specimens and integrated the data to obtain stress-strain plots of rock materials. The analysis results showed that the experimental samples were in dynamic stress equilibrium with constant strain rate during most of the impact damage.

JuYang et al <sup>[32]</sup> studied the deformation, fragmentation, and energy dissipation characteristics of porous rocks under stress waves using the separated Hopkinson pressure bar (SHPB) system and simulated them numerically.

Based on the modified Hopkinson system, Li Xibing et al <sup>[33]</sup> et al. conducted impact damage experiments on rock specimens with different dynamic-static combined loading to analyze the fragmentation law, strength characteristics, and energy absorption efficiency of the specimens. It was obtained that when the dynamic load impact is certain and the axial static pressure is loaded to 70% of the uniaxial static strength of the specimen, the maximum strength of the rock with combined dynamic and static loading is obtained.

Guo Deyong et al <sup>[34]</sup> used separated SHPB compression rods to impact coal samples with different impact velocities, and the collected data were used to analyze the strain rate changes, damage characteristics and other patterns of the specimens to establish a viscoelastic damage intrinsic model of coal.

Ying Zhang et al <sup>[35]</sup> conducted dynamic impact experiments on rocks using  $\phi 50$ mm Hopkinson rods, and the results of analyzing the dynamic stress-strain curves showed that the damage strength of rocks increased with the increase of strain rate, and there was an obvious strain rate effect.

Pengpeng Zhang et al <sup>[36]</sup> obtained the parameters of the HJC intrinsic model of coal body based on the mechanical parameters of Huainan coal mine, referring to the literature data of other scholars, and used Ls-Dyna software to numerically simulate the coal SHPB active peritectic pressure experiment.

Chengwu Li et al <sup>[37-39]</sup> used the HJC intrinsic structure model in Ls-Dyna software to numerically simulate the coal Hopkinson rod passive surround pressure experiment and impact damage experiment, and compared the experimental results with good similarity; and used the HHT analysis processing method to denoise the measured coal dynamic impact damage signal, which has a significant effect on high frequency signal separation.

Bin Wang et al <sup>[40]</sup> used a modified  $\phi 75$  mm SHPB rod for impact damage experiments on sandstone with different water contents to analyze the effect of water on the dynamic damage strength of sandstone.

Yaqi Zhang et al <sup>[41]</sup> conducted dynamic loading and combined dynamic-static loading experiments on dolomite specimens using a modified triaxial Hopkinson rod to analyze the effect of dynamic loading static loading on rock crushing strength according to the crushing morphology of the rock.

Liyun Li et al <sup>[42]</sup> conducted SHPB impact damage experiments on sandstone specimens with a combination of dynamic and static compression to compare and analyze the energy absorption of the two loading states. The results showed that the static compression consumed more energy than the dynamic compression for sandstone specimens producing the same damage pattern.

Liu Junzhong et al <sup>[43]</sup> tested the dynamic mechanical properties of hornblende specimens at different strain rates using large-size detached Hopkinson rods, and

obtained the relationship between the dynamic compressive strength of hornblende, etc., and the average strain rate.

Deng Jian et al <sup>[44]</sup> used Fourier transform waveforms to study the response and energy dissipation of rocks under random stress waves and found that the harder the rock, the less energy it absorbs.

Xie Beijing et al <sup>[45-47]</sup> considered the porous media properties of coal, the weakening effect of gas on the coal body, and determined the range of HJC parameters of coal through experiments to simulate the coal Hopkinson rod impact damage process, which is in good agreement with the comparison of experimental test results; and studied the variation characteristics of the experimental magnetic field of coal Hopkinson rod impact damage.

Baochen Liu et al <sup>[48]</sup> obtained empirical formulas by analyzing rock uniaxial compression test data and studying the size effect of rock compressive strength.

Yang Shengqi et al <sup>[49,50]</sup> proposed a model for the size effect of rock materials and concluded that the frictional effect on the end face is responsible for the size effect of the material.

Li F. et al <sup>[51]</sup> numerically simulated the dynamic damage process of coal pillars based on the HJC intrinsic structure model in LS-DYNA software, and the results showed that the damage energy of coal pillars was related to the strain rate.

Wang Dengke et al <sup>[52]</sup> conducted impact damage tests on coal samples from the Reed Town Mine with different impact loads, and the results showed that both the elastic modulus and compressive strength of coal showed a positive correlation with the strain rate.

Wang Runping and others <sup>[53]</sup> conducted force-controlled uniaxial compression experiments on coal samples to study the dynamic damage time during coal impact damage, and concluded that the damage time of coal is a comprehensive reflection of coal stiffness strength.

Song Honghua et al <sup>[54]</sup> studied the effect of inhomogeneous distribution of the internal structure of coal samples on the damage morphology of coal under uniaxial compression conditions.

Li Xibing et al <sup>[55-57]</sup> used finite element calculations to construct punches for the Hopkinson rod device and conducted simulation verification experiments to improve the design of large diameter SHPB tests; Hopkinson rod was used to study rock crushing theory by combined dynamic and static loading method.

Scholars of dynamic mechanical properties of the materials research process, most of them only consider the damage results of materials under the action of single impact damage, ignoring that the damage of coal rock body in actual engineering is sometimes due to the accumulation of different intensity energy impact, such as cumulative damage in the form of impact ground pressure, the fragmentation of underground coal rock body is under the action of multiple damage impact to produce damage, and finally lead to fragmentation. Therefore, it is necessary to study the dynamic mechanical properties of materials under cyclic impact damage.

---

### **1.2.2 Research status of cyclic damage evolution and dynamic load failure of coal and rock materials**

---

In the process of underground mining, affected by the disturbance of excavation and change of ground stress, there will be rock-burst, coal rock dynamic damage and other disasters. If the early warning and prevention is not timely, these disasters will often cause casualties, property losses, environmental damage and a series of adverse consequences. The occurrence of rock burst and other damage phenomena is often due to the multiple changes of stope stress field and the multiple impacts of different energy on coal and rock, resulting in damage evolution, crack expansion, and finally crushing occurrence of disasters and accidents. Many scholars have studied and analyzed the damage evolution effect of coal and rock mass under cyclic loading and the mechanism of coal and rock dynamic disaster.

Jingjing Zhu et al <sup>[58]</sup> used the SHPB test device to analyze the damage law of granite under cyclic impact loading, and the results showed that the yield strain of the specimen increased with the increase of the number of impacts, and the damage became more severe.

Wang Zhiliang et al <sup>[59]</sup> conducted cyclic impact experiments on black mica granite using the SHPB device, and four different stress wave incident amplitudes exhibited different damage laws.

Xiao-Long Song et al <sup>[60]</sup> used geological radar to study the damage evolution effect of blasting on tunnel surrounding rock, and the results showed that the damage effect of surrounding rock was negatively correlated with the distance of cyclic blasting point.

Jin Peijian et al <sup>[61]</sup> used servo pressure testing machine to study the change law of electromagnetic radiation of coal rock damage process under cyclic loading conditions, and the results showed that the change law of electromagnetic radiation was influenced by the friction effect of crack evolution load coal rock matrix in the process of breaking phantom.

Liu Yongjie et al <sup>[62]</sup> built an experimental system independently to study the change law of surface potential signal of cyclic loading damage of gas-bearing coal.

Shaohe Liu et al <sup>[63]</sup> used the SHPB experimental platform with enclosing pressure device to conduct cyclic impact experiments on sandstone specimens under uniaxial and triaxial conditions, analyzed the stress-strain characteristics of sandstone under cyclic impact loading, and analyzed the relationship between ultrasonic wave velocity and stress-strain.

Yu Yang et al <sup>[64]</sup> conducted cyclic impact tests on sandstone using a Hopkinson impact device with enclosing pressure and concluded that the damage factor of sandstone was positively correlated with the average strain rate and showed regularity with the increase of enclosing pressure.

Bing Dai et al <sup>[65]</sup> conducted damage evolution experiments on granite using the SHPB device and concluded that the damage accumulation showed a positive correlation with the average strain rate and the accumulation ratio energy absorption value increased with the increase of impact number.

Lin Danneng et al <sup>[66,67]</sup> used a pressure testing machine to impact load marble specimens and concluded that the presence of surrounding pressure could improve the bearing capacity of the rock and reduce the damage rate.

Xu Qian <sup>[68]</sup> performed cyclic impact experiments on sandstone specimens using a SHPB device with an enclosing pressure, and calculated the propagation distance of the impact wave within the sandstone by analyzing the curve.



Jin Jiefang et al <sup>[69]</sup> concluded that the cyclic impact stress-strain curves of rocks can be divided into five stages, these are compressional density, elastic deformation, crack expansion and two decompression stages.

Li Nan et al <sup>[70]</sup> derived the variation law of the main frequencies of the initial sound of rock loading, unloading stage, constant load stage and rupture stage during cyclic loading.

Xianbin Yu et al <sup>[71]</sup> established a dual elastic modulus instantonal model using a device that can perform uniaxial compression and tension experiments simultaneously.

The previous studies on the cyclic impact damage evolution of materials are mostly on hard materials such as rocks and concrete, and there are relatively few studies on coal; there are more studies on the damage evolution of materials under uniaxial conditions, and relatively few studies on the cyclic impact damage evolution of materials under triaxial envelope pressure conditions. Therefore, it is necessary to conduct experimental and numerical simulation studies on the cyclic impact damage evolution characteristics of coal under triaxial envelope pressure conditions.

---

## **1.3 Research contents and methods**

---

### **1.3.1 Main research contents**

---

In this paper, experimental testing, theoretical analysis and data analysis are combined.

(1) Through the customized SHPB impact test platform under triaxial confining pressure, the cyclic loading impact test and corresponding comparative test were carried out on the processed coal samples under triaxial confining pressure, and the impact failure characteristics of coal samples under different loading conditions were compared and analyzed;

(2) The stress wave propagation law of cyclic impact coal sample is analyzed, the damage evolution law of coal body is obtained, and the damage evolution mechanism and cumulative damage form of coal body are studied;

(3) The stress-strain and strain rate characteristics of confined coal under different damage and impact times and impact speed are analyzed to determine the damage, failure law and mechanical characteristics of coal under triaxial confining pressure;

---

### **1.3.2 Research methods and technical route**

---

This study mainly adopts the method of field experimental test and data analysis to conduct the impact damage experiments of coal Hopkinson pressure bar (SHPB) with the different number of cyclic impacts, different crushing impact velocities, and with or without surrounding pressure conditions, and through the analysis of stress wave propagation law and crushing morphology of the specimen, the damage evolution characteristics and dynamic mechanical characteristics of the specimen are derived. It provides the experimental basis and theoretical basis for studying the damage mechanism of coal body cyclic impact dynamic load, the damage mechanism of impact ground pressure, and the prevention and early warning of coal-rock dynamic disaster occurrence. The specific technical route is shown in Fig. 1.1.

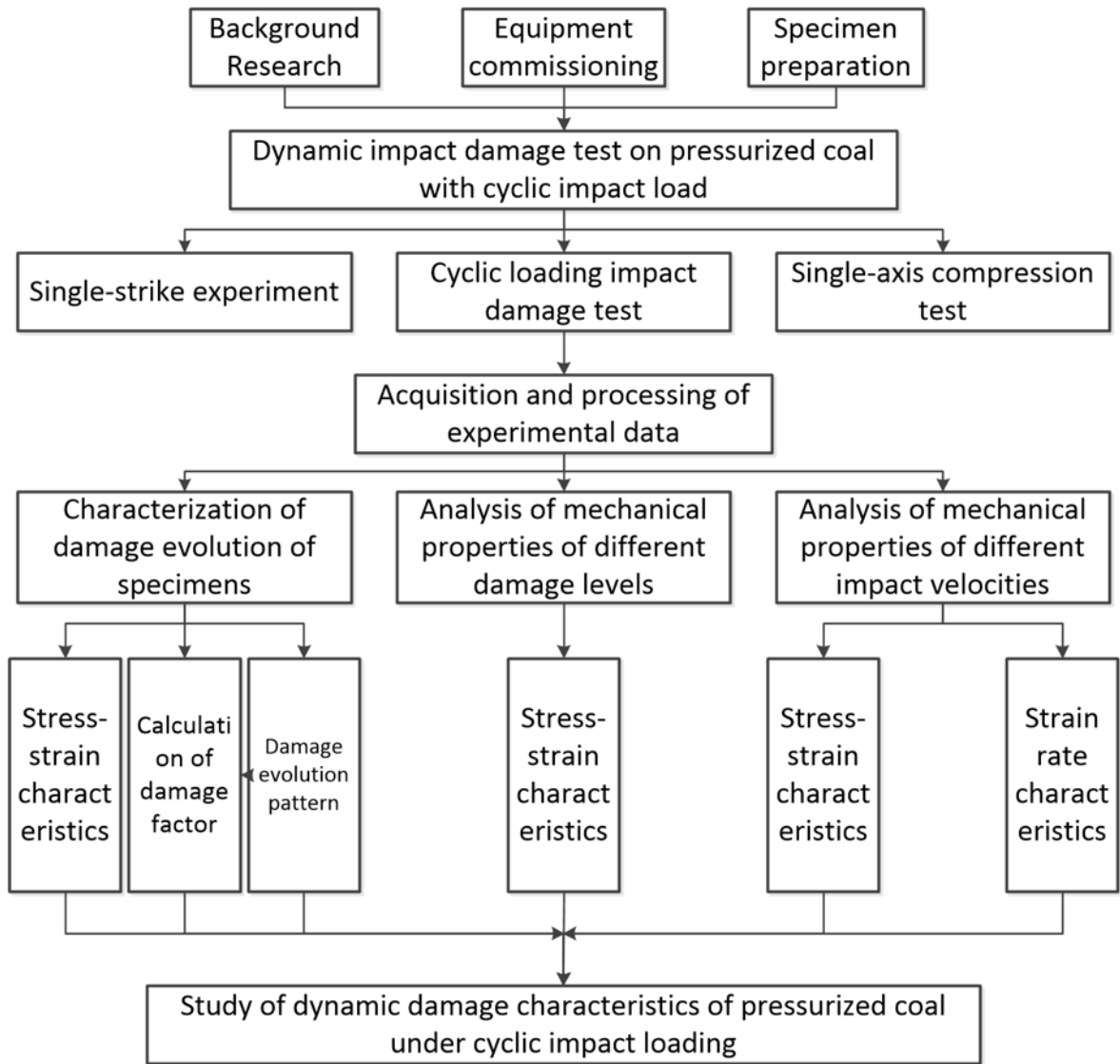


Fig. 1.1 The specific technical route

---

## **2 Dynamic impact failure system and experiment of confined coal under cyclic impact load**

---

### **2.1 Introduction**

---

With the rapid development of engineering field and mining field, the available resources and space in the shallow layer of the surface are less and less, the development of deep space and the exploitation of resources tend to be normal, and the rock mechanics problems are increasingly complex [72-78].

The dynamic mechanics of materials can be studied from three aspects: theoretical analysis, experimental research and numerical simulation. Because the process involved in the dynamic mechanics of materials is completed in an instant, experimental research is the main means of dynamic mechanics. To observe and record these processes and phenomena, we must rely on scientific experiments. In practical engineering, such as rock burst, rock-burst, roof fall and other disasters and accidents have the characteristics of sudden. Therefore, it is necessary to study the mechanism of these dynamic phenomena and the damage law of materials with the help of scientific experiments.

This chapter mainly introduces the cyclic loading triaxial confining pressure dynamic load failure experiment and the experimental system composition, sample preparation and impact failure results of the sample. The measured data provide the analysis basis for the damage evolution effect of coal and the dynamic mechanical characteristics of coal.

---

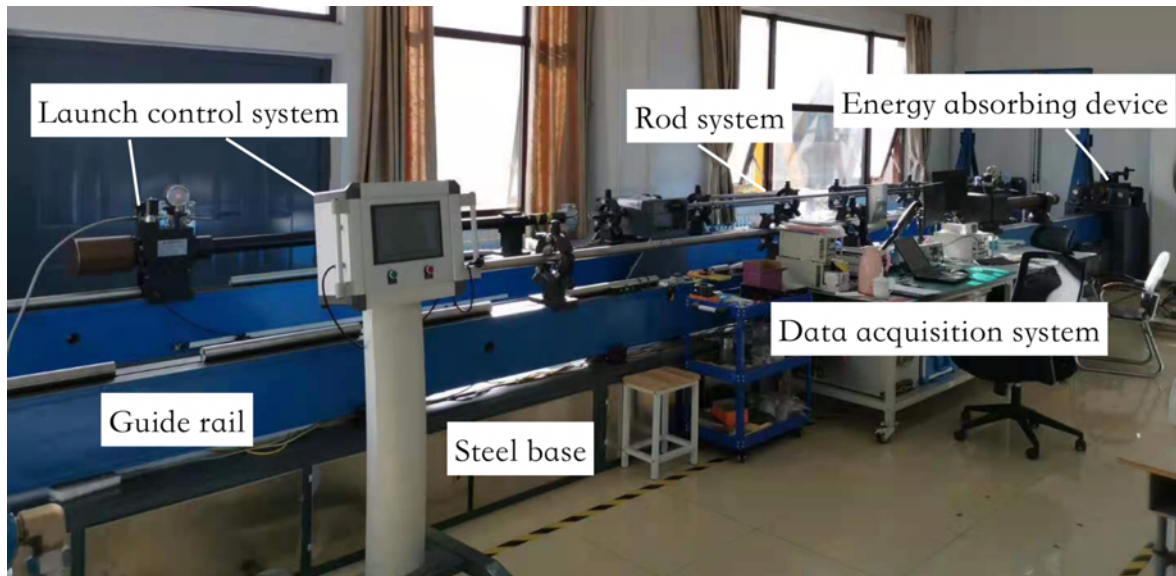
### **2.2 Impact failure system of triaxial confining pressure dynamic load**

---

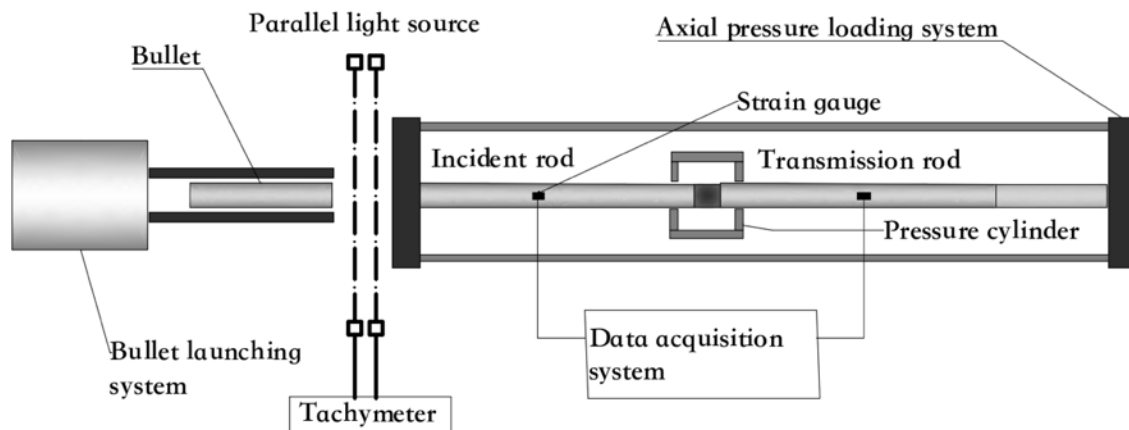
The dynamic impact test of cyclic loading coal under triaxial confining pressure was carried out on the triaxial confining pressure dynamic impact test platform in Shahe campus of China University of Mining and Technology (Beijing).

The system consists of rod system, bullet launching system, confining pressure loading system, data acquisition system, limit device system, steel base and guide

rail, air-source system and energy absorbing device. The physical diagram of the device is shown in Fig. 2.1 (a), and the schematic diagram is shown in Fig. 2.1 (b).



(a) The physical diagram



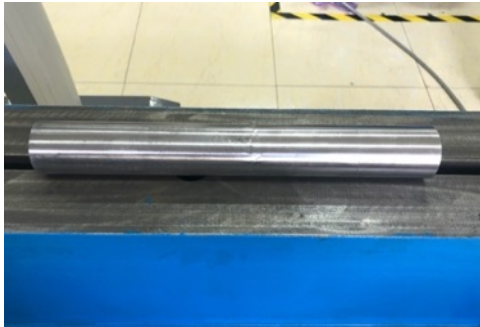
(b) The schematic diagram

Fig. 2.1 SHPB device picture

The rod system consists of a  $\Phi 50 \times 3000$ mm  $\Phi 50 \times 2500$ mm transmission rod. The material of the bar is spring steel, the straightness of the bar is 0.05mm/m, the perpendicularity of the end face is 0.02, the surface finish is 0.8, and the yield strength is more than 1300Mpa.

The bullet launch system is  $\Phi 50$ mm bullet, as shown in Fig. 2.2 (a), automatic PLC control system, bullet launching device, and launching chamber. The automatic PLC control system consists of a solenoid valve and a 10 inch LCD touch screen console, as shown in Fig. 2.2 (b), with a control accuracy of 0.1MPa and two red and green

entity emission buttons. The bullet launching device, as shown in Fig. 2.2 (c), includes launching and control part, solenoid valve, sensor, pressure gauge, piston, support, adjusting valve, etc. The inner diameter of the firing chamber is 50 mm, as shown in Fig. 2.2 (d), the yield strength is greater than 500 MPa, the straightness is 0.05 mm / m, and the firing speed of the bullet can reach 3-50 M/s.



(a)  $\Phi 50\text{mm}$  bullet



(b) 10 inch LCD touch screen console



(c) Bullet launching device



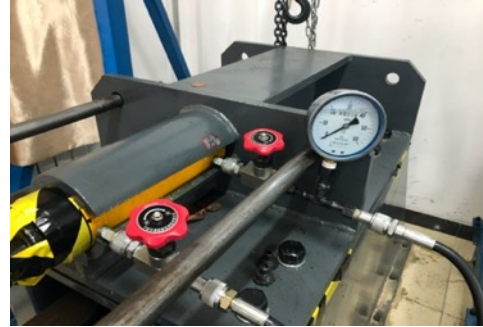
(d) Firing chamber

**Fig. 2.2 Launch control system**

The confining pressure digital loading system is composed of confining pressure cylinder as shown in Fig. 2.3 (a), axial pressure loading system as shown in Fig. 2.3 (b) and automatic closed-loop electro-hydraulic servo loading system as shown in Fig. 2.3 (c). The volume of the confining pressure cylinder is 2.5L, the maximum radial pressure is 50MPa, and it is equipped with a rubber sleeve, fixed structure, and shockproof pressure gauge. The pressure chamber of the confining cylinder produces radial pressure on the sample. The pressurized medium is hydraulic oil, and the pressurized power source is a motor. The maximum pressure can be 6 MPa. If the pressure needs to continue, it needs to be pressed in by a manual pressure rod. The pressure can be observed by a pressure gauge.



(a) The pressure cylinder



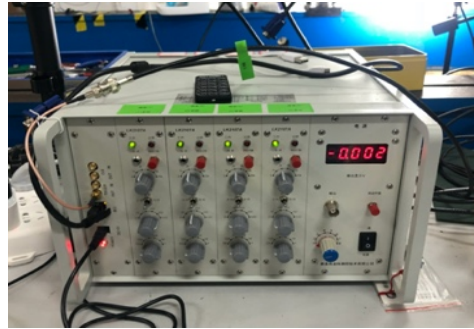
(b) Axial pressure loading system



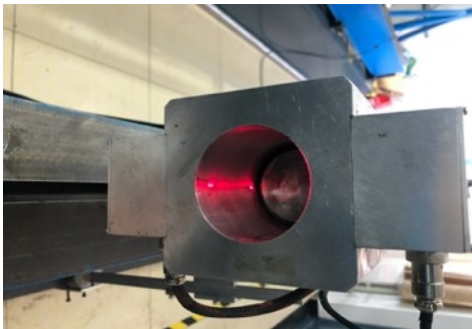
(c) Automatic closed-loop electro-hydraulic servo loading system

**Fig. 2.3 Digital loading system for ambient pressure**

The data acquisition system consists of a super dynamic strain gauge and a Hopkinson special non-contact optical velocimeter, in which the ultra-dynamic data acquisition instrument consists of a 4-channel data acquisition system. Two channels are used in the experiment to connect strain gauges attached to the incident rod and transmission rod, as shown in Fig. 2.4 (a). The Hopkinson special non-contact optical velocimeter is composed of optical sensing structure and digital display velocimeter. The optical sensing part adopts a sleeve structure, which can be perfectly combined with the bullet launching chamber. The resolution of the LCD screen of the digital display velocimeter is 128x64, the speed range is 0-100m / s, the test precision is 0.001m/s, the crystal frequency is 24MHz, the high sensitivity device is adopted, the low value of reaction time is 0.2ns, the precision is 0.5  $\mu$ s , as shown in Fig. 2.4 (b).



(a) The ultra-dynamic data acquisition instrument



(b) SHPB special non-contact optical velocimeter

**Fig. 2.4 Data acquisition system**

The limiting device system consists of an entrance rod limiter, as shown in Fig. 2.11 (a), an axial pressure limiting rod, as shown in Fig. 2.12 (b), and a central frame, which is used to limit the displacement of the rod when loading the axial pressure, to ensure that the sample is not squeezed and the accuracy of the experiment.



(a) Entrance rod limiter



(b) Axial pressure limiting rod

**Fig. 2.5 Limit device system**

The center frame is composed of a base, three-way adjusting bracket with bearing, sliding limit damper, confinement nut, etc. by adjusting each component, the support and movement of members can be ensured in the same center. The adjustment range of the sliding limit damper is  $\Phi 37\text{mm} \sim \Phi 75 \text{ mm}$ , as shown in Fig. 2.6.



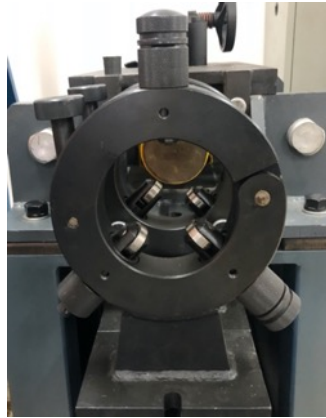


**Fig. 2.6 The center frame**

The steel base is equipped with a guide rail connection and adjusting block to adjust the height and horizontal position. The material of the guide rail is cast iron, the surface is precision machined, the straightness is 0.08mm/m, and the guide rail surface is provided with a T-shaped groove, which can quickly install and adjust the launcher, center frame, buffer device, etc. under a unified reference, as shown in Fig. 2.7.



**Fig. 2.7 Steel base and guide rail**

The energy absorption device can absorb the impact energy produced by the impact of the bar in the uniaxial compression experiment. The size of the energy absorption damping is adjusted by the damping wheel. as shown in Fig. 2.8.



**Fig. 2.8 The energy absorption device**

The air source used in the impact test is provided by DEJURA DJ-0.8/40 air compressor, which is driven by a three-phase asynchronous motor. The rated power is 11kw, the flow rate of the compressor is 0.8m<sup>3</sup>/min, the discharge pressure is 4.0Mpa, the maximum working pressure of the air tank is 4.4mpa, and the total volume is 0.32m<sup>3</sup>. It is equipped with pressure reducing valve and gas path connecting pipe. As shown in Fig. 2.9.



**Fig. 2.9 Air compressor**

---

## **2.3 dynamic impact failure experiment of coal under triaxial confining pressure under cyclic impact load**

---

### **2.3.1 SHPB experimental principle**

---

The principle of the SHPB experiment is based on the theory of elastic stress wave propagation in a slender bar. The stress-strain relationship of the specimen material is deduced by measuring the strain on the compression bar. Two basic assumptions followed in the SHPB experiment are the one-dimensional stress assumption of elastic compression bar and stress homogenization assumption of specimen [79].

The one-dimensional stress assumption considers that each cross-section of the elastic rod always keeps a plane state during the propagation of the stress wave in the slender rod; Stress homogenization assumes that the stress in the specimen is equal everywhere.

The experimental principle of SHPB is shown in Fig. 2.10 [80],  $\varepsilon_i(t)$  is the incident wave generated by bullet impact,  $\varepsilon_r(t)$  is the reflected wave formed by the incident wave on the contact surface between the incident rod and the specimen, and  $\varepsilon_t(t)$  is the transmission wave formed by the incident wave passing through the specimen,

which is collected by the strain gauges on the incident rod and the transmission rod. E, C and A are the elastic modulus, longitudinal wave velocity, and cross-sectional area of the incident or transmitting rod respectively.

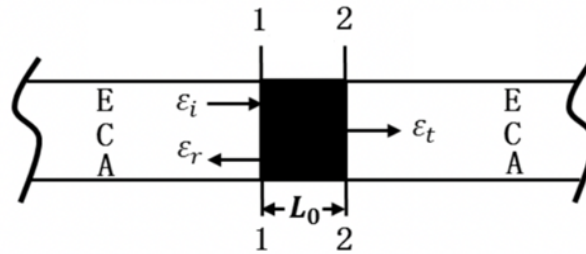


**Fig. 2.10 The experimental schematic diagram of SHPB**

According to the assumption of stress uniformity, the strain rate, stress, and strain of the sample can be calculated by combining the formula (2.1), (2.2), and (2.3), where  $A_0$  and  $l_0$  are the cross-sectional area and thickness of the specimen. The strain rate time curve and stress-strain curve of the specimen is drawn by the calculated results.

$$\dot{\epsilon}_s = \frac{2C}{L_0} \epsilon_r(t) \quad (2.1)$$

$$\epsilon_s(t) = \frac{2C}{L_0} \int_0^t \epsilon_r(t) dt \quad (2.2)$$

$$\sigma_s(t) = \frac{AE}{A_0} \epsilon_i(t) \quad (2.3)$$

To ensure that the collected data is processed more accurately, the SHPB rod system is calibrated before processing the data. That is, to determine the proportionality  $K$  between the strain of the rod and the measured voltage  $U$  obtained by the direct impact of a bullet with a certain initial velocity ( $v_0$ ) on the rod without adding a specimen.

The bullet impact velocity is  $v_0$  then the stress formula of the rod is Equation (2.4), where  $\rho_0$ ,  $C_0$ ,  $v_0$  are the density of the rod, the ultrasonic velocity of the rod, and the bullet impact velocity, respectively. According to the formula of elastic modulus of the rod as  $E = \rho_0 C_0^2$  and the formula of stress-strain relationship (2.5), the formula

of empty rod strain can be calculated as formula (2.6), and finally the ratio formula of strain to voltage  $K = \frac{\varepsilon}{U}$  can be derived.

$$\sigma = -\frac{1}{2}\rho_0 C_0 v_0 \quad (2.4)$$

$$\varepsilon = \frac{\sigma}{E} \quad (2.5)$$

$$\varepsilon = -\frac{v_0}{2C_0} \quad (2.6)$$

---

### 2.3.2 Preparation and testing of specimens

The small-size model test suffers from size effects, i.e., different stress-strain characteristics exist for specimens with different aspect ratios under the same test conditions <sup>[51,81]</sup>. The SHPB dynamic impact experiments follow the assumption of one-dimensional stress waves and the assumption of stress-strain uniformity, so it is necessary to choose a suitable length-to-diameter ratio to fully satisfy these two assumptions, and many scholars have conducted a series of studies on this issue.

In the literature <sup>[82]</sup>, dynamic impact damage experiments were performed on five sets of sandstone specimens with aspect ratios of 0.4, 0.5, 0.6, 0.8 and 1. By analyzing the degree of specimen fragmentation and the stress-strain curve, it was concluded that the dynamic damage strength of the rock showed a positive correlation with the increase in the aspect ratio of the specimens, and the range of aspect ratios of sandstone for Hopkinson compression bar experiments was derived from the analysis.

The literature <sup>[83]</sup> suggested that porous brittle materials have low impedance to stress waves, and the specimen is too thick will affect the uniformity of stress distribution, so the length-to-diameter ratio should not be chosen too large.

The scholars chose a large range of length-to-diameter ratios for SHPB experimental specimens, combined with the conclusions of previous studies and in accordance with the processing requirements of rock mechanics specimen materials. In order to make a better comparison between the uniaxial compression and triaxial compression load experimental results, the length-to-diameter ratio of

the specimen is 1, i.e., the specimen is machined into  $\phi 50 \text{ mm} \times 50 \text{ mm}$  size, and the verticality of the end face is less than 0.02.

The coal body specimens used in the experiment were taken from Xinzhou City, Shanxi Province, and a total of 22 specimens were selected for display in this test, including 16 cyclic impact specimens YM-1--YM-16 (Fig. 2.11), 4 single impact specimens YM-17--YM-20 (the names were changed to DC-1--DC-4 when processing the data for easy differentiation) and two single-axis compression high-speed camera shots specimens GS-1--GS-2 (Fig. 2.12).

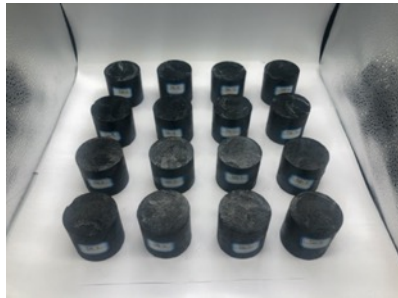


**Fig. 2.11 Cyclic impact specimen**



**Fig. 2.12 Single impact and single-axis compression specimens**

Industrial analysis of the coal body, solidity coefficient, true and false density, porosity, adsorption constant  $a_b$  value, and other basic parameter tests are mailed to the North China Institute of Science and Technology for measurement. The automatic industrial analyzer, gas diffusion velocity meter, automatic density meter and gas adsorption constant meter used are shown in Fig. 2.13. The specific numerical results of the measurements are shown in Table 2.1.



(a) Automatic industrial analyzer



(b) Gas diffusion velocity meter



(c) Automatic density meter



(d) Gas adsorption constant measuring instrument

Fig. 2.13 Test equipment for coal sample foundation parameters

Tab. 2.1 Basic parameters of coal body

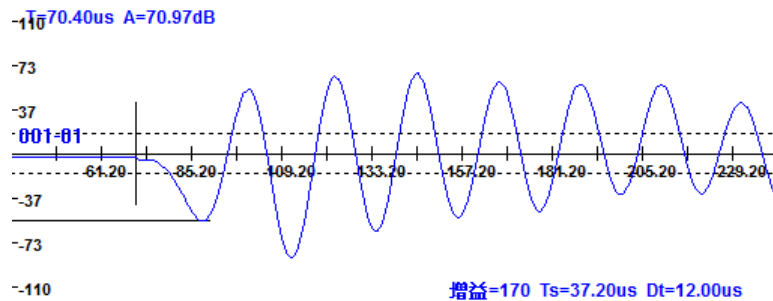
Parameters	Value	Notes
Gas Discharge Initial Velocity (mL/s)	14.3	
Solidity coefficient	0.98	Greater than the prominence critical value 0.5, the coal body is more stable
Moisture content (%)	2.91	
Volatile content (%)	23.13	Ash and volatile content are high, coal quality belongs to bituminous coal
Ash content (%)	14.67	
Fixed carbon content (%)	59.28	
Absorption constant (cm <sup>3</sup> /g·r)	34.33	
Absorption constant (MPa <sup>-1</sup> )	0.249	
True density (t/m <sup>3</sup> )	1.5831	The difference between true density and apparent density of the sample is not big, and the value of porosity is small, which means the structure of coal body is more stable and uniform
Apparent density (t/m <sup>3</sup> )	1.5173	
Porosity (%)	4.16	

As shown in Table 2.1, it can be seen from the results of the industrial analysis that the volatile matter and ash content of the coal are relatively high, the coal quality belongs to the category of bituminous coal, the solidity coefficient is large, which indicates that the coal is hard and the coal structure is stable, the difference between the true density and apparent density values is not large, and the porosity values are small, which also indicates that the coal structure is relatively uniform and stable, and the specimens meet the requirements of SHPB dynamic impact damage experiments.

The greater the ultrasonic wave velocity of the coal sample, the denser the coal body is, and vice versa, indicating that the coal body structure may have certain fissures. The test was conducted using the ZBL-U5100 non-metallic ultrasonic detector produced by the ZBL company for 22 specimens, and the test equipment and test results are shown in Figure 2.14. The diameter and height of the specimen were measured with an electronic vernier caliper accurate to the hundredth percentile, and the mass of the specimen was measured with an electronic pallet balance accurate to the thousandth percentile.



(a) Non-metallic ultrasonic velocimetry



(b) Ultrasonic test result

Fig. 2.14 Ultrasonic testing equipment and test results

The ultrasonic test methods for the specimens are:

- (1) Adjust the parameters of the non-metallic ultrasonic detector and set the parameter data matching the specimen to be tested.
- (2) The two ends of the specimen will be evenly coated with petroleum jelly, the purpose is to make close contact between the specimen end face and the ultrasonic probe to improve the accuracy of the measurement.
- (3) will transmit and receive a non-metallic ultrasonic probe attached to the two ends of the specimen, gently pressed by hand to ensure effective contact between the probe and the two ends of the specimen.
- (4) operation of the detector, press the "sampling" button, wait for the detector screen to display waveform stability, press the "store" button, the operation is complete.

The experiment set up the ZBL-U5100 non-metal ultrasonic detector with three test points, as shown in Figure 2.20(b), and the instrument averaged the test results of the three test points to get the final test results. The height, diameter, mass and ultrasonic test results of the specimen, as well as the group number, are shown in Table 2.2.

**Table 2.2 Basic parameters of samples**

<b>Specimen number</b>	<b>Height(mm)</b>	<b>Diameter (mm)</b>	<b>Weight(g)</b>	<b>Ultrasonic speed (km/s)</b>
XH-1	49.90	49.44	129.130	1.50
XH-2	50.09	49.40	135.082	1.75
XH-3	49.46	49.44	138.545	1.97
XH-4	49.91	49.45	140.361	1.78
XH-5	49.42	49.53	140.060	1.77
XH-6	49.85	49.46	136.836	1.82
XH-7	49.76	49.46	137.273	1.51
XH-8	49.68	49.44	136.591	1.97
XH-9	50.12	49.58	145.803	1.64
XH-10	49.16	49.48	134.876	1.69
XH-11	49.49	49.48	131.412	1.69
XH-12	49.44	49.43	139.298	1.88
XH-13	49.50	49.77	136.642	1.64
XH-14	49.75	49.48	137.741	1.97
XH-15	50.06	49.52	138.545	1.60



XH-16	49.97	49.47	134.812	1.56
DC-1	50.04	50.01	141.009	1.41
DC-2	51.20	49.20	139.548	1.40
DC-3	50.02	48.98	128.994	1.39
DC-4	50.00	49.52	128.972	1.56
GS-1	50.06	49.36	129.122	1.42
GS-2	50.02	48.96	137.889	1.48

In order to more clearly demonstrate the distribution pattern of the basic parameters of each specimen, the mass of the specimen and ultrasonic wave velocity are plotted as a line graph, as shown in Figure 2.15. For the convenience of plotting, the 22 specimens are shown in the figure in the order of the table from top to bottom with numbers 1-22.

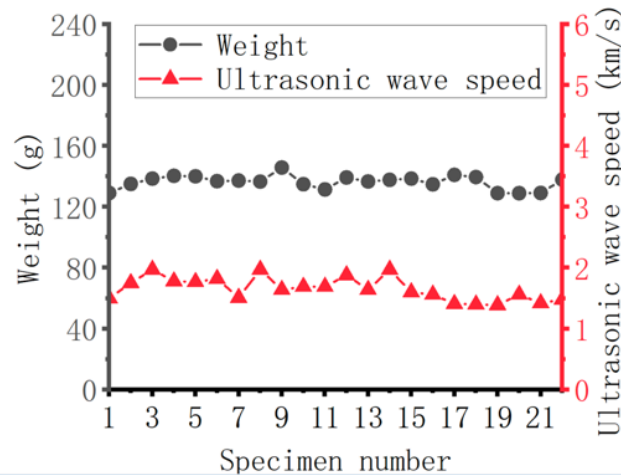


**Fig. 2.15 Distribution chart of specimen parameters**

From Table 2.2 and Figure 2.15 can be seen that the weight of the 22 specimens in the 128.818 ~ 145.803g, fluctuations in the range of about 15g, the height and diameter difference of no more than 2mm, ultrasonic wave velocity between 1.40 ~ 1.97km / s, the difference is small, indicating that the 22 specimens are more uniform texture, no large cracks, in line with the basic requirements of the dynamic impact damage test.

### 2.3.3 Experimental steps

The 22 specimens were divided into three groups, the first group XH-1 -- XH-16 was the cyclic impact load triaxial circumferential compression SHPB impact damage experimental group, DC-1 -- DC-4 single impact triaxial circumferential compression SHPB control experimental group, GS-1 -- GS-2 was the uniaxial compression

SHPB high-speed camera control experimental group. In order to comply with the two hypotheses of the SHPB experiment and to fully ensure the reliability of the experimental results, the SHPB experiment should first ensure that the experimental equipment is in a horizontal state before the SHPB experiment, that is, the rod system is calibrated horizontal, which is the most basic and critical step. The impact of 0.2 MPa air pressure was the damaging impact, and the last impact of the specimen was the crushing impact. The design scheme of the three sets of experiments is shown in Table 2.4.

**Table 2.4 Experimental design scheme**

<b>Specimen number</b>	<b>Cyclic loading scheme (MPa)</b>	<b>Specimen number</b>	<b>Cyclic loading scheme (MPa)</b>
XH-1	0.2+0.8	XH-9	0.2+1.2
XH-2	0.2+0.2+0.8	XH-10	0.2+0.2+1.2
XH-3	0.2+0.2+0.2+0.8	XH-11	0.2+0.2+0.2+1.2
XH-4	0.2+0.2+0.2+0.2+0.8	XH-12	0.2+0.2+0.2+0.2+1.2
XH-5	0.2+1.0	XH-13	0.2+1.4
XH-6	0.2+0.2+1.0	XH-14	0.2+0.2+1.4
XH-7	0.2+0.2+0.2+1.0	XH-15	0.2+0.2+0.2+1.4
XH-8	0.2+0.2+0.2+0.2+1.0	XH-16	0.2+0.2+0.2+0.2+1.4
<b>Specimen number</b>	<b>Single blow intensity /MPa</b>	<b>Specimen number</b>	<b>Impact strength /MPa</b>
DC-1	1.4	GS-1	0.2
DC-2	1.2	GS-2	0.8
DC-3	1.0		
DC-4	0.8		

As can be seen from Table 2.3, the experimental variables of the cyclic impact loading triaxial circumferential pressure SHPB impact damage experimental group are the number of damage impact loading and the strength of the dynamic load damage impact, with the purpose of studying the damage evolution effect of cyclic impact and the effect of different impact velocities on the dynamic mechanical properties of the coal body. The bullet inflation pressure of the damage impact was 0.2 MPa, and the 16 cyclic impact specimens were divided into four groups, group 1 XH-1 -- XH-4, group 2 XH-5 -- XH-8, group 3 XH-9 -- XH-12, and group 4 XH-13 - - XH-16. The overall variable between the four groups was the magnitude of the last impact air pressure of the specimen, which was 0.8 MPa, 1.0 MPa, 1.2 MPa and

1.4 MPa, respectively, in order to analyze the law of impact pressure and the degree of dynamic impact crushing of the specimen. The variables within each group are the number of 0.2 MPa damage impacts of the specimens, which are 1, 2, 3 and 4 times, respectively, in order to analyze the damage evolution law of dynamic impact damage of coal body materials under triaxial envelope pressure conditions. The single-impact triaxial perimeter pressure experiment was used as a control group with the cyclic impact condition, in which the inflation pressures of the single-impact bullets were 0.8 MPa, 1.0 MPa, 1.2 MPa, and 1.4 MPa, respectively. The single-axis compression experiment considered the perimeter pressure to be "zero" as a control group with the triaxial perimeter pressure condition, and the single-axis compression. The inflation pressure of the experiments was 0.2MPa and 0.8MPa, and the high-speed camera was used to record the percussion crushing process.

The steps of the triaxial pressure SHPB dynamic impact damage test are as follows:

- (1) Level and calibrate the launch chamber, incidence rod, transmission rod and absorption rod so that the rods are at the agreed level, and install the enclosing pressure cylinder between the incidence rod and transmission rod to adjust them to be at the agreed level with the rod system.
- (2) Install the axial pressure loading device, the incidence rod limiter and the axial pressure limiting rod to ensure that the rod system does not produce displacement when axial pressure is added.
- (3) Attach strain gauges to the incidence rod and transmission rod respectively, connect the data acquisition instrument and calibrate the strain gauges.
- (4) Push the bullet into the firing chamber, clamp the specimen coated with molybdenum disulfide at both ends between the two rods, push it into the perimetric cylinder and fix the specimen.
- (5) Connect the PLC control system, automatic closed-loop electro-hydraulic servo loading system, velocimeter and air inlet system.
- (6) The automatic closed-loop electro-hydraulic servo loading system loads the axial radial pressure of the required value, and the air inlet system flushes in the set gas pressure.

(7) Check whether the systems are connected correctly to ensure that the data acquisition system is operating properly.

(8) Control the bullet firing, and the data acquisition system records the required data.

(9) Unload the axial radial pressure and remove the specimen.

(10) Repeat the above experimental steps until all specimens are loaded and destroyed.

Single-axis compression high-speed camera experiments do not need to enclose the pressure-related operational steps, after the rod is leveled in the appropriate location set up high-speed camera, set the appropriate trigger switch, with a transparent glass cover wrapped around the specimen to prevent the splash out of the debris damage to the camera, other steps and enclose the same pressure experiments.

---

## **2.4 Experimental results of dynamic impact damage of triaxial pressure coal with cyclic impact loading**

---

### **2.4.1 Uniaxial compression specimen crushing results**

---

The uniaxial compressed coal SHPB impact damage experiments were performed with impact air pressures of 0.2 MPa and 0.8 MPa and impact velocities of 4.611 m/s and 9.988 m/s, respectively, with the aim of comparing the effects of triaxial pressure conditions on specimen crushing under the same impact air pressure. The uniaxial compression dynamic damage process of GS-1 and GS-2 was recorded by a high-speed camera, and the captured uniaxial compression impact video was cut out to show the impact damage process of the specimen with representative pictures, as shown in Figure 2.20 and 2.21. The left end of the specimen in the figure is the incident rod and the right end is the transmission rod.

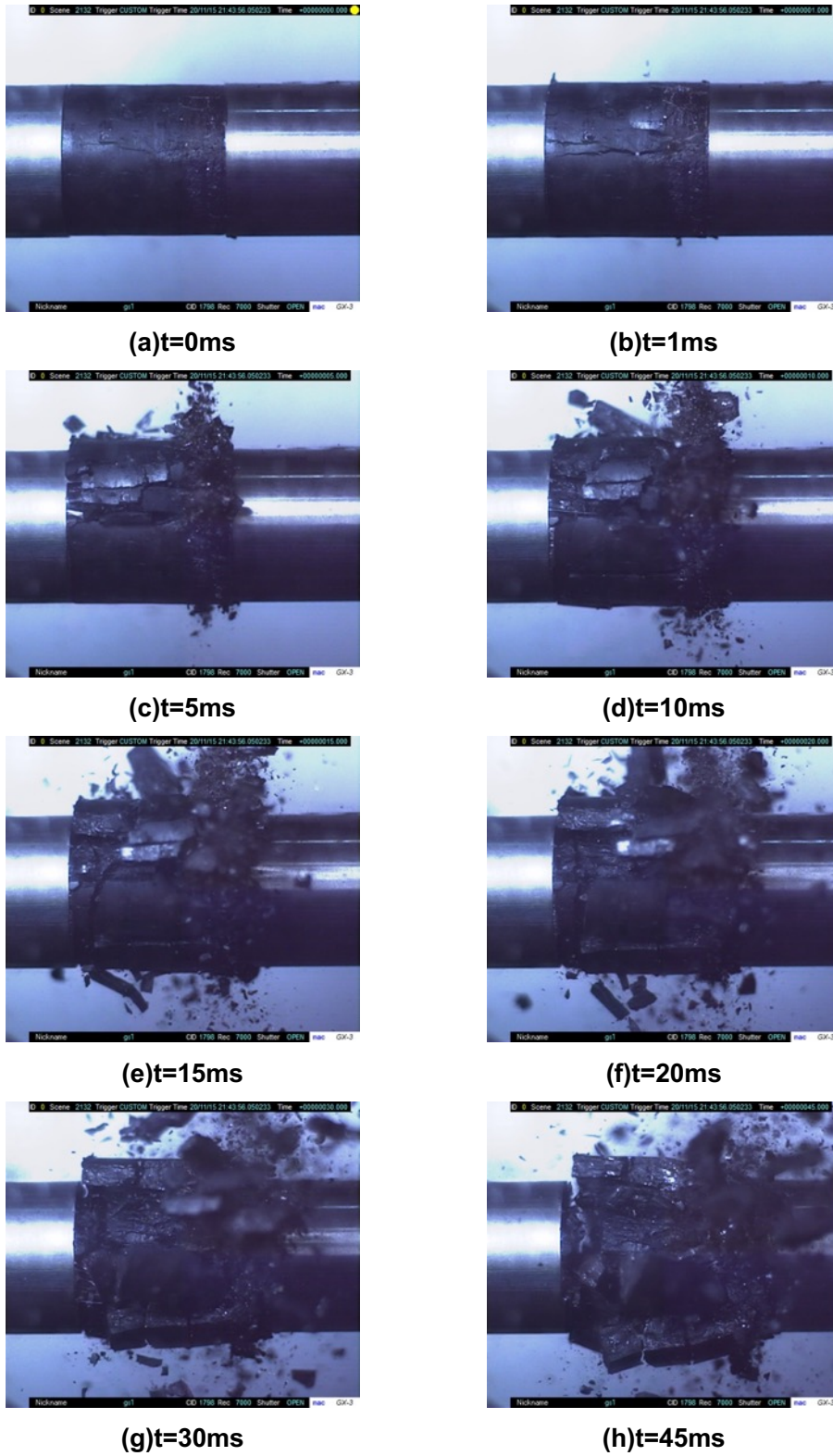
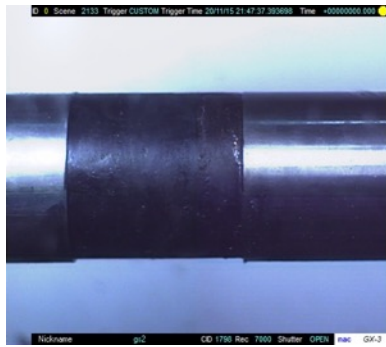
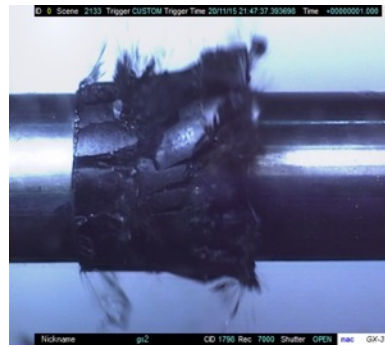


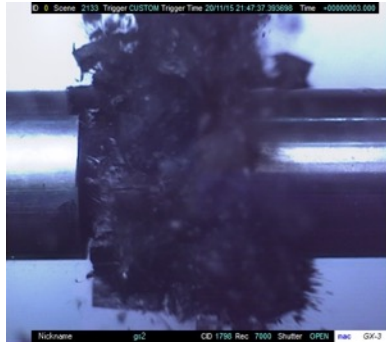
Fig. 2.20 4.611m/s impact process diagram



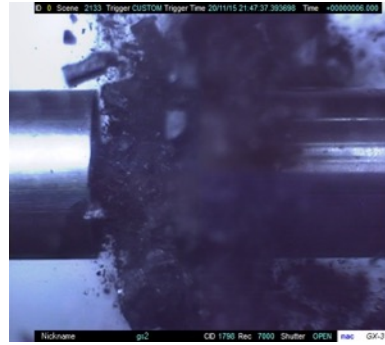
(a)t=0ms



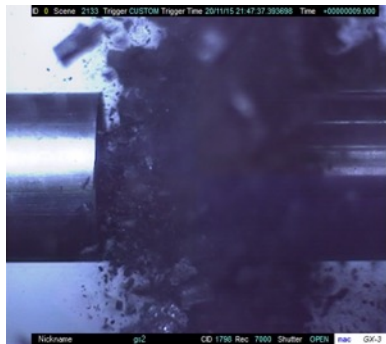
(b)t=1ms



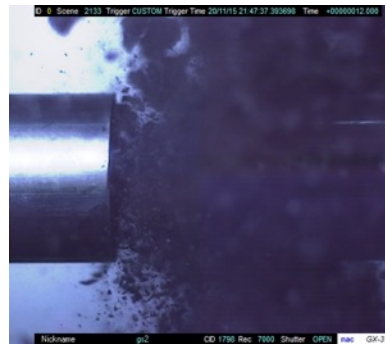
(c)t=3ms



(d)t=6ms



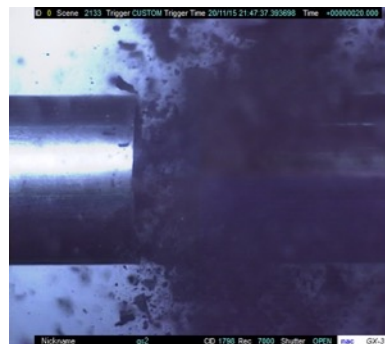
(e)t=9ms



(f)t=12ms



(g)t=15ms



(h)t=20ms

Fig. 2.21 9.988m/s impact process diagram



(a) GS-1



(b) GS-2

**Fig. 2.22 Uniaxial compression fracture results of specimens**

From Figure 2.20, it can be seen that when the specimen is compressed uniaxially at an impact velocity of 4.611 m/s, axial cracking starts to appear in the specimen when the stress wave first arrives as shown in Figure 2.20(a). With the expansion of the crack, the end away from the incident rod begins to break as shown in Figure 2.20(b), followed by a certain expansion and deformation of the specimen, in which the expansion and deformation phenomenon is more obvious near the end of the transmission rod. The specimen starts to appear fully broken from the right end to the left end as shown in Fig. 2.20(c-h) until it is completely broken, and the fragments are in the form of bulky lumpy particles with the block size gradually decreasing from left to right. It indicates that the impact air pressure of 0.2 MPa and bullet velocity of 4.611 m/s is sufficient to completely crush the specimen under the condition of no surrounding pressure. Figure 2.21 is the picture of the crushing process of the specimen when the specimen is compressed uniaxially at an impact speed of 9.988m/s. The specimen does not show macroscopic cracks when the stress wave is first transmitted as shown in Figure 2.21(a). The reason for the analysis is that the specimen is initially subjected to the compression-density phase due to the squeezing action, and the coal body accumulates energy and then deforms by expansion. The crushing phenomenon starts to appear near the end of the transmission rod as shown in Figure 2.21(b). Then the crack gradually expanded and the specimen started to show full crushing phenomenon from the right end to the left end as shown in the figure until it was completely crushed, as shown in Figure 2.21(c-h). Under the condition of no surrounding pressure, the impact air pressure of 0.8 MPa and bullet velocity of 9.988 m/s can make the specimen crushingly broken.

Figure 2.22 shows the crushing results of uniaxial compression high-speed camera experimental specimens GS-1 and GS-2. Compared with 0.2 MPa impact air pressure, the crushing size of the specimens under 0.8 MPa impact air pressure is smaller, the crushing phenomenon occurs faster and the crushing effect is more obvious.

In order to ensure the success of the experiment and avoid the specimens being damaged by a single blow, two specimens processed from the same batch were selected for the pre-impact experiments in the experimental design. Under the same experimental conditions as the cyclic loading experiment, the specimens were loaded with the impact air pressure of 0.2 MPa and 0.3 MPa, and the corresponding bullet impact velocities were 4.632 m/s and 5.452 m/s, respectively, and no crushing or cracking was found on the removed specimens. The ultrasonic velocimeter was used to measure the two specimens, and the measured values were slightly larger than the ultrasonic values of the specimens before the impact, indicating that there was no crack expansion inside the specimens. It proves that the impact air pressure of 0.2MPa and 0.3MPa cannot break the specimens by impact under certain triaxial circumferential pressure conditions. Comparing the crushing results of the specimens without surrounding pressure shows that the surrounding pressure under certain conditions improves the load-bearing capacity of the specimens, and the existence of surrounding pressure can significantly reduce the damage of the specimens under the same damage impact air pressure.

---

#### **2.4.2 Triaxial pressure specimen crushing results**

The results of the cyclic impact loading triaxial pressure coal SHPB impact damage experiment and the single strike triaxial pressure coal SHPB impact damage experiment are shown in Figure 2.23. The specimen loading parameters, strain rates, and crushing patterns are summarized in Table 2.5. The first 16 images in Figure 2.23 show the results of cyclic impact loading triaxial pressure coal SHPB impact damage experiments, and the last four images show the results of single strike triaxial pressure coal SHPB impact damage experiments.

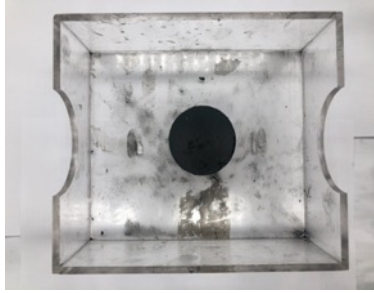




**XH-1**



**XH-2**



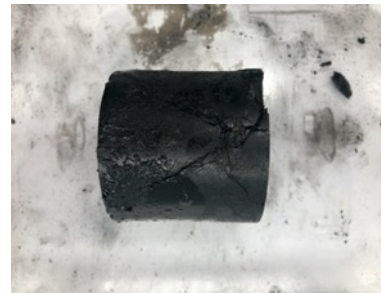
**XH-3**



**XH-4**



**XH-5**



**XH-6**



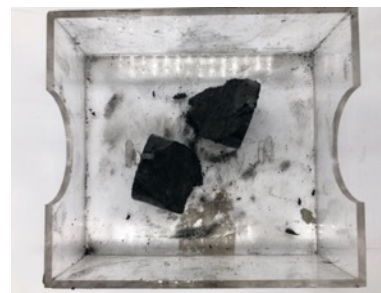
**XH-7**



**XH-8**



**XH-9**



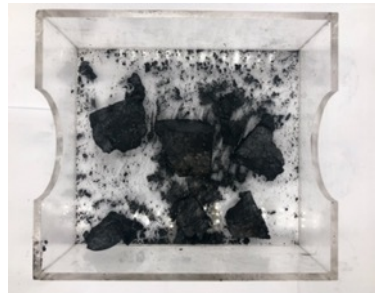
**XH-10**



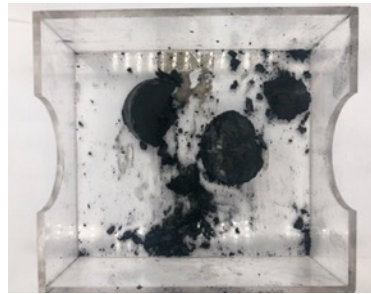
XH-11



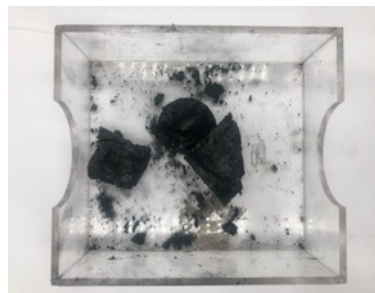
XH-12



XH-13



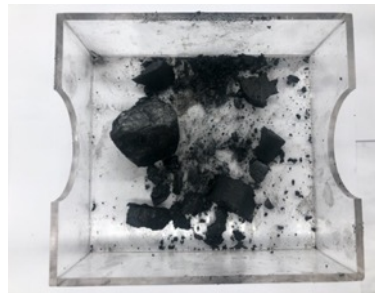
XH-14



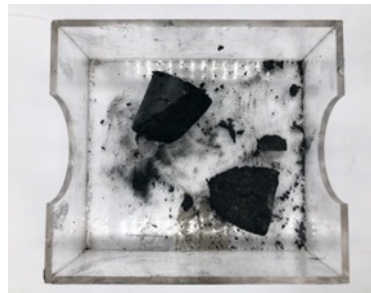
XH-15



XH-16



DC-1



DC-2



DC-3



DC-4

Fig. 2.23 SHPB dynamic impact failure results of coal under cyclic impact confining pressure

Table 2.5 Loading parameters and failure forms of samples

Specimen number	Number of the damaging impacts	Crushing impact air pressure (MPa)	Crushing impact speed (m/s)	Failure forms
XH-1	1	0.8	Not detected	Cracks
XH-2	2	0.8	9.850	Larger cracks
XH-3	3	0.8	9.982	Smaller cracks
XH-4	4	0.8	9.944	Cracks
XH-5	1	1.0	11.140	Large pieces
XH-6	2	1.0	11.003	Larger cracks
XH-7	3	1.0	Not detected	Cracks
XH-8	4	1.0	10.936	Cracks
XH-9	1	1.2	12.019	Large pieces
XH-10	2	1.2	12.051	Large pieces
XH-11	3	1.2	12.156	Cracks
XH-12	4	1.2	12.083	Large pieces
XH-13	1	1.4	13.000	Crushed, less small pieces
XH-14	2	1.4	13.058	Crushed, less small pieces
XH-15	3	1.4	13.071	Large pieces
XH-16	4	1.4	13.068	Large pieces
DC-1		1.4	13.142	Crushed, less small pieces
DC-2		1.2	12.189	Large pieces
DC-3		1.0	11.052	Large pieces
DC-4		0.8	10.014	Larger cracks
GS-1		0.2	4.611	Crushed
GS-2		0.8	9.988	Crushed

The overall damage of the cyclic impact specimen with the increase in the number of damage impact degree shows a trend of first decreasing and then increasing. The degree of damage of a single impact specimen tends to increase gradually with the increase of impact air pressure.

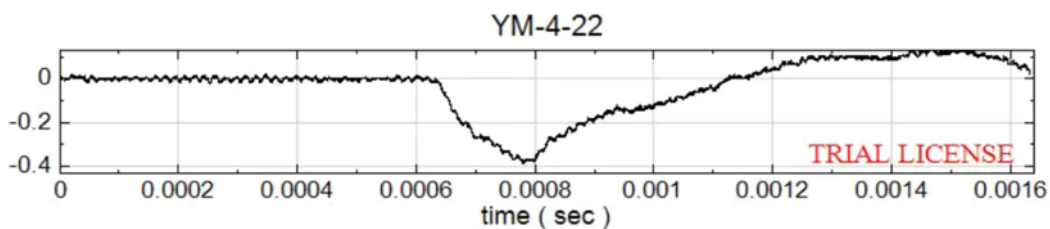
Comparing specimens DC-4 and GS-2, under the same crushing impact, the degree of crushing of uniaxial compression specimens is much greater than that of specimens under triaxial enclosure pressure. It indicates that the enclosing pressure improves the bearing capacity of the specimens within a certain range, and the

existence of the enclosing pressure can significantly reduce the damage of the specimens.

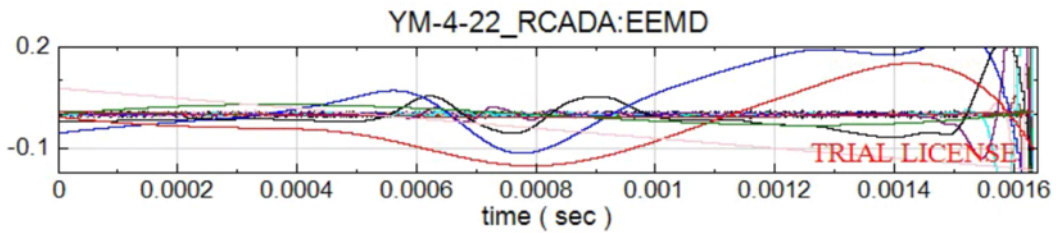
## 2.5 High-frequency noise reduction processing of the signal

The experimental site is affected by outdoor noise, indoor load equipment, radio communication equipment and other different types of disturbances, and the collected voltage signal will have high-frequency noise. The HHT method of the DATADEMON software was used to perform high-frequency noise reduction on the raw voltage signals collected by the hyperdynamic strain gauge to obtain incident, transmitted, and reflected signals without high-frequency disturbance of the SHPB dynamic shock damage<sup>[47]</sup>. The core of the HHT high-frequency noise processing method is the empirical mode decomposition, that is EMD, which is based on the characteristic time scale to identify all vibration modes contained in the signal and decompose them into multiple groups of single-component signals IMF. the decomposed IMF components are combined, the high-frequency components are discarded and the normal components are retained to finally obtain the voltage signal with high-frequency noise removed<sup>[47]</sup>.

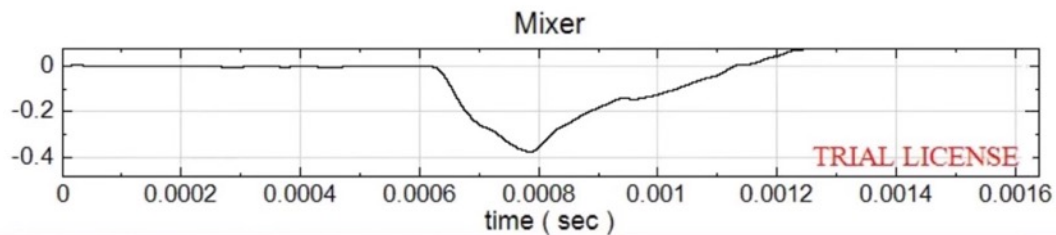
Figure 2.24(a) shows a typical transmissive voltage signal collected by a super dynamic strain gauge. It can be seen that the curve is subject to obvious high-frequency perturbations and sawtooth fluctuations, and the accuracy of the calculated stress-strain curve will be affected if this signal is not processed for noise reduction. Figure 2.24(b) shows the combination of the effective IMF components decomposed by the HHT method of the DATADEMON software, and the curves of the recombination of the IMF components after noise reduction are shown in Figure 2.24(c). It can be seen that the curve after EMD decomposition and IMF component recombination, the high-frequency noise elimination effect is obvious in the case that the overall trend of the signal is consistent with the original curve.



(a) Original voltage signal



(b) Each IMF component that is decomposed



(c) Signal curve after high frequency-noise removal

Figure 2.24 Noise processing of voltage signals

## 2.6 Summary of the chapter

This chapter introduces the dynamic load impact damage experiments of cyclically loaded triaxial pressure coal and the impact damage platform for the related comparison experiments, and the experiments are designed according to the experimental purpose and the related principles of SHPB experiments. A specific experimental procedure is developed, and the specimens required for the experiments are prepared according to the experimental needs, the results of the SHPB damage experiments are shown, and finally the noise reduction processing method for high frequency noise signals is described.

(1) The triaxial circumferential compression SHPB compression rod test system can realize the specimen axial radial circumferential compression dynamic load impact damage, the system consists of rod system, bullet firing system, circumferential compression loading system, data acquisition system, limit device system, rigid base and guide, air source system and energy absorption device.

(2) The experimental scheme of cyclic loading triaxial coal SHPB impact damage and the corresponding control experimental scheme were designed, and specific experimental steps were developed.

(3) Twenty-two raw coal specimens with an aspect ratio of 1 were selected according to the experimental requirements, including 16 cyclic impact specimens

YM-1--YM-16, 4 single impact specimens DC-1--DC-4 and two single-axis compression high-speed camera shot specimens GS-1--GS-2.

(4) The damage results of the dynamic load impact damage experimental specimens of cyclically loaded triaxially enclosed coal are shown and the damage morphology of the specimens is described. Comparing the crushing morphology of uniaxial compression test and triaxial enclosure test specimens under the same impact air pressure, it is concluded that the triaxial enclosure compression under certain conditions can improve the bearing capacity of the specimens. Under the same damage impact pressure impact damage, the degree of fragmentation of the specimens without perimeter pressure is much higher than that of the specimens with perimeter pressure, and the existence of perimeter pressure can significantly reduce the damage of the specimens.

(5) The method of removing the high frequency-noise of the disturbed voltage signal is described.

### **3 Analysis of dynamic impact damage evolution characteristics of pressurized coal under cyclic impact loading**

---

#### **3.1 Introduction**

---

At present, there are two main experimental research methods for rock mechanics, the first one is to study the static mechanical properties of rock materials by using loaded specimens such as servo presses, and the other one is to study the dynamic mechanical properties of rock materials by using equipment that can produce dynamic impact damage such as Hopkinson rods, light air cannons and falling hammer devices. The difference between these two experimental methods lies in the different mechanical states applied to the materials, i.e., static and dynamic loads. These two experimental research methods have achieved quite a lot of research results. However, in engineering practice, most materials are subjected to mechanical loads in a combined dynamic and static manner, i.e., the materials themselves are subjected to static loads before they are damaged by the impact of dynamic loads. Such as tunnel excavation, mine excavation, etc., coal and rock materials are subjected to high ground stress static load at the same time also subjected to dynamic load, which is a typical combination of dynamic and static loading of materials. In recent years this type of problem has received the attention of many scholars, and relevant research has been conducted to reach conclusions.

This chapter combines the basic concepts of damage mechanics and previous research results, and takes specimens XH-4, XH-8, XH-12 and XH-16, which have experienced four damage impacts, as the research objects. The damage evolution variables of triaxially enclosed compressed coal are determined, and the damage evolution stress-strain characteristics of the specimens are analyzed to provide a basis for the following study of dynamic mechanical properties of compressed coal under cyclic impact loading.

### 3.2 Selection of damage variable

Determining the damage variable  $D$  (degree of damage) is a fundamental step in the study of material damage. The correct damage variable has 2 main characteristics.

(1) Has a high accuracy damage description that shows the main damage characteristics of the material.

(2) contains fewer defined parameters and is easy to calculate.

Defining damage variables is the basis for determining the relationship between the mechanical properties of a material and its structure. When defining damage variables of materials, it is more important to pay attention to the real damage characteristics of materials while considering engineering applications. The damage characteristics of a material determine the characteristics of the changes in the molecular structure and physical properties of the material, i.e., macroscopic and microscopic, so the damage variables can be defined in these two aspects [84].

In terms of the molecular structure of the material, the damage of the material can be determined from the area, shape, distribution mode and number of defects of the material, etc. There are four common methods of definition.

(1) Micro-defect area to define  $D$

As the area of micro-defects produced by the damage effect material becomes  $A_D$ , define the cross-sectional area of the material at this time as  $A$ , then the damage variable  $D$  of the material can be defined as:

$$D = A_D / A \quad (3.1)$$

(2) Micro-defect volume to define  $D$

Chinese scholars Wu Gang et al [85] used the volume of microdefects to define the damage variable:

$$D = V_D / V \quad (3.2)$$

Where  $V_D$  is the volume of microdefects and  $V$  is the volume of the matrix. The definition of damage variables by volume has a clear meaning and few parameter



variables at the theoretical level, but it is not convenient for practical use because the volume of the damage body in the rock mass cannot be quantitatively calculated.

(3) The number of microdefects to define D

The number of microdefects can also be used to define the damage variable [86,87], and scholars have used the ratio of the number of damaged microelements to the total number of microelements to define the damage variable by taking advantage of the different kinds of distributions that the intensity of microelements obeys.

$$D = n / N \quad (3.3)$$

(4) Fractal method to define D

From the perspective of fractal damage of materials, some scholars believe that the damage of materials show fractal characteristics, and the change of fractal dimension can be used to indicate the change of the degree of material damage. From the fractal dimension to determine the average size of the material  $\alpha$  crack impact range.

$$N = \beta \alpha^{-D_f} \quad (3.4)$$

The expression for the crack density is given by:

$$C_d = \beta \alpha^{3-D_f} \quad (3.5)$$

According to the relationship between the damage variable D and the crack density  $C_d$ , we can obtain:

$$D = \frac{161 - v^2}{91 - 2v} \beta \alpha^{3-D_f} \quad (3.6)$$

Where  $D_f$  is the fractal dimension. After equations (3.4) and (3.5) the damage variables can be expressed in terms of fractal dimensions.

In terms of physical properties of materials, parameters such as modulus of elasticity, ultrasonic wave velocity, density and volume, mass density, energy, magnitude of stress-strain, and magnitude of yield stress can usually be selected.

(1) Defining D based on the modulus of elasticity

Lamaitre used the undamaged elastic modulus and the post-damaged elastic modulus to define the damage variables [88]:

$$D = 1 - \frac{E_n}{E_1} \quad (3.7)$$

where  $E_n$  is the modulus of elasticity of the specimen after the  $n$ th impact and  $E_1$  is the modulus of elasticity of the specimen after the 1st impact.

(2) Define  $D$  based on ultrasonic wave velocity

After the damage of the specimen internal fissures, ultrasonic wave propagation speed and undamaged ratio will become slower. Take the specimen that has been processed without impact as a nondamaged specimen, and the specimen that has been damaged by impact as a damaged specimen, then the damage variable of the specimen can be expressed as:

$$D = 1 - \left(\frac{C_n}{C_0}\right)^2 \quad (3.8)$$

Where  $C_n$  is the ultrasonic wave velocity value of the specimen after the  $n$ th test, and  $C_0$  is the original ultrasonic wave velocity value of the specimen. NDT technology has been fully developed, so the method of using ultrasonic wave velocity to define the damage variable has the advantages of simple and convenient operation, time and effort saving, and small impact on the material.

(3) Define  $D$  based on the change of density and bulk density

The degree of damage to the material can also be expressed in terms of density and capacitance, and according to the law of conservation of mass,  $D$  can be expressed as:

$$D = 1 - \psi = -\frac{\Delta\rho}{\rho_0} \quad (3.9)$$

(4) Based on energy to define  $D$

According to the laws of thermodynamics, it is known that the process of deformation and damage of materials must produce energy dissipation, reflected in the development of internal cracks in the material, the process of gradually increasing damage. The greater the degree of damage the higher the intensity of

energy dissipation. Xie and Ping [89] defined the energy damage variables of the rock material unit:

$$\omega = \frac{U^d}{U^c} \quad (3.10)$$

Where  $U^c$  is the critical energy dissipation energy and  $U^d$  is the unit dissipation energy.

(5) Defining D based on strain

Foreign scholars have defined damage variables based on strain:

$$D = \left(\frac{\varepsilon}{\varepsilon_s}\right)^n \quad (3.11)$$

Where  $\varepsilon$  is the axial strain,  $\varepsilon_s$  is a constant,  $n$  is the material brittleness parameter, the larger the value of  $n$ , the more brittle the material is.

From equation (3.11), it can be seen that the damage is a function of strain, and the change in strain state determines the damage evolution and is related to the damage state.

(6) Based on CT number variation to define D

With the vigorous development of computer technology, computerized laminar identification techniques have received more and more attention from scholars of rock mechanics. In the application of CT technique in material damage detection, Yang Ganshe [90] gave an expression to calculate the damage variables based on CT number.

$$D = \frac{1}{m_0} \left(1 - \frac{1000 + H_{rm}}{1000 + H_{rm0}}\right) \quad (3.12)$$

Where  $m_0$  is the CT machine resolution,  $H_{rm}$  is the CT number of the specimen at a certain damage state.

There are various methods for defining damage variables. The measurement of damage variable parameters defined from the microscopic point of view is more complicated, and the calculation of the amount of microdefects in the specimen requires the use of high-precision measuring instruments, so the microscopic

definition method is discarded. From the macroscopic variable point of view, the damage variable is quantitatively determined. Since this experiment was designed for triaxial enclosing pressure conditions, the changes in parameters such as ultrasonic wave velocity and density tolerance after each blow of the specimen were not measured to ensure constant enclosing pressure conditions and to avoid damage to the specimen during disassembly and loading. Instead, the changes in the elastic modulus of the specimen after each blow could be calculated from the stress-strain curve.

In this paper, the definition of damage variables is chosen based on the modulus of elasticity, i.e., Equation (3.7) is used to calculate the damage degree of the specimen after each damage impact. This can ensure the constant triaxial circumferential pressure conditions and also avoid the damage to the specimen during disassembly and loading, define the damage variables of the specimen more precisely, and calculate the cumulative damage of the specimen.

---

### **3.3 Study of damage evolution characteristics of coal**

---

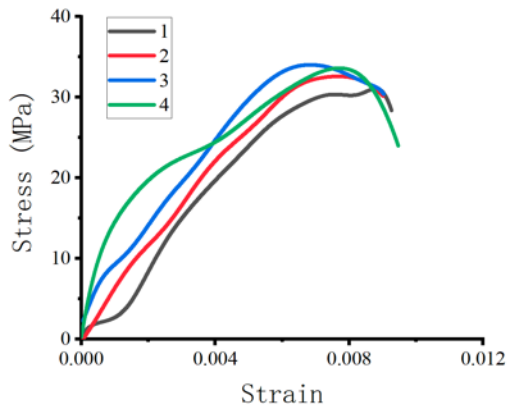
#### **3.3.1 Specimen damage evolution stress-strain curve analysis**

---

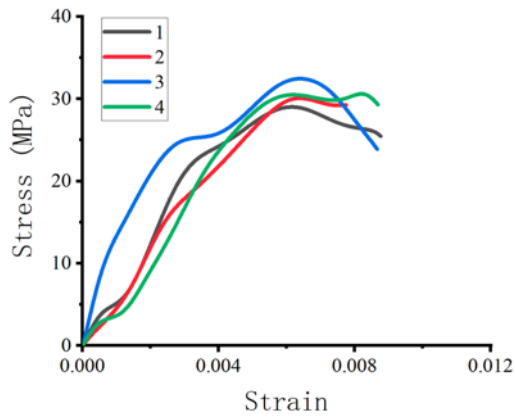
After applying high-frequency noise processing to the voltage signal data collected by the hyperdynamic data acquisition instrument using DATADEMON software, the stress-strain correlation curves of the specimens were calculated and plotted by combining equations (2.1), (2.2) and (2.3) in Chapter 2 and the calibrated K values of the experimental system rods.

According to the experimental design, the dynamic impact damage of SHPB with 0.2 MPa air pressure was defined as damage impact. Figure 3.1 shows the stress-strain curves of the damage impact of cyclic impact load specimens under triaxial enclosing pressure condition, the enclosing pressure condition is fixed as the axial pressure is set to 10 MPa and the radial enclosing pressure is set to 15 MPa. 4 groups of specimens experienced 4 damage impacts, and the stress-strain curves of the specimens after each damage impact are shown in the figure. the trend of the stress-strain curves of the 4 groups of damage evolved specimens is basically the same, and the stress-strain curve reaches After reaching the peak stress, the stress-strain curves showed a rebound phase, indicating that the specimens did not

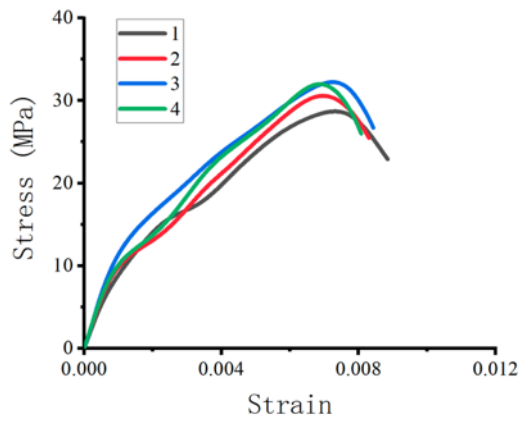
undergo macroscopic damage, and the rebound was due to the release of elastic energy of the specimens during stress unloading.



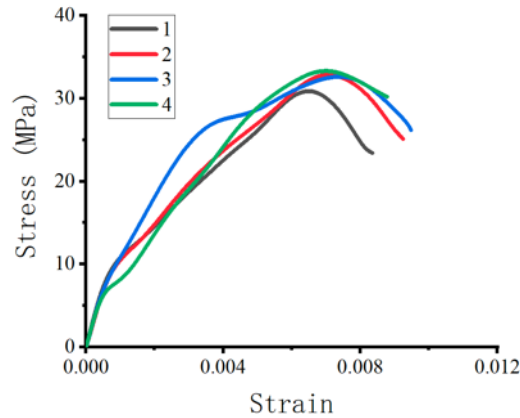
(a) Stress-strain curve of XH-4 4 times damage impact



(b) Stress-strain curve of XH-8 4 times damage impact



(c) Stress-strain curve of XH-12 4 times damage impact



**(d) Stress-strain curve of XH-16 4 times damage impact**

**Fig. 3.1 Stress-strain curve of specimen damage evolution**

Figure 3.1(a) shows the stress-strain curves of specimen XH-4 under the effect of four cycles of impact damage evolution. The stress-strain curves of the specimen for the four impacts are basically the same, with the increase of the number of cycles of impact, the maximum stress that the specimen can withstand shows a trend of first increasing and then decreasing, with the peaks of 31.06MPa, 32.58MPa, 34.01MPa and 33.50MPa respectively. The peak stresses of the stress-strain curves of the specimens in the 1st, 2nd and 3rd impacts gradually increased, and the peak stresses of the stress-strain curves of the specimens in the 4th impact were smaller than those in the 3rd and larger than those in the 1st and 2nd impacts. From the viewpoint of strain, the strain magnitude of the specimen showed a trend of decreasing and then increasing under the same magnitude of stress near the peak stress, and the strain in the peak stress region of the specimen gradually decreased in the first three impacts and increased in the fourth impact. This indicates that the strength of the specimen increases and then decreases with the increase of the number of cyclic impacts.

Figure 3.1(b) shows the stress-strain curves of specimen XH-8 under the effect of four cycles of impact damage evolution, with the increase of the number of cycles, the peak stresses of the specimens show a trend of increasing and then decreasing, which are 29.02 MPa, 30.08 MPa, 32.45 MPa and 30.59 MPa, respectively. The peak stresses of the first three impacts gradually increase, and the peak stresses of the fourth impact specimens are smaller than those of the third impact. The peak stress of the fourth impact specimen was smaller than the third impact. The strain size showed a trend of decreasing and then increasing.

Figure 3.1(c) shows the stress-strain curves of specimen XH-12 under the action of 4 cycles of impact damage evolution, with the increase of the number of cycles, the peak stresses to which the specimen was subjected showed a trend of first increasing and then decreasing, the peak stresses of each impact were 28.69 MPa, 30.57 MPa, 32.45 MPa and 31.94 MPa, respectively. The strength of the specimens increased and then decreased, and the strength of the specimens after the 4th impact was greater than that after the 1st impact, and the strength of the specimens after the 4th impact was greater than that of the specimens at the 1st impact, demonstrating a pattern that was in good agreement with that of the first two sets of cyclic impact specimens.

Figure 3.1(d) shows the stress-strain curves of specimen XH-16 under the action of four cycles of impact damage evolution, and the peak stress magnitudes of each impact are 30.88 MPa, 32.63 MPa, 32.85 MPa and 33.32 MPa, respectively. The peak stress of specimen XH-16 showed a tendency to increase gradually with the increase of the number of cycles. The strain near the peak stress showed a decreasing trend, indicating that the strength of the specimen increased with the increase of the number of impacts.

The distribution laws of the stress-strain graphs of the four groups were generally consistent, and the first three groups showed better distribution regularity. There were two main reasons for analyzing the distribution laws of the stress-strain graphs of the cyclic impact specimens of the first three groups.

(1) Analyzed from the perspective of microscopic cracks in the coal body, the molecular structure of the coal body itself determines the dense type of molecular arrangement of the coal body, and there are original microscopic cracks in the coal. When the coal body is subjected to dynamic impact, the energy transmitted by the impact damage can make the microscopic cracks close and become more dense<sup>[91]</sup>, leading to an increase in the impedance effect of the specimen on the stress wave. The first three dynamic shocks produce less damage to the specimen than the amount of microscopic crack closure within the material, so the impedance effect of the material on the wave increases, leading to a gradual increase in the peak stress of the stress-strain curve. When the microscopic fracture closure is complete, the impact damage to the coal body again, the impact load will act on the original fracture, causing the stress concentration of the original fracture, causing

macroscopic crack expansion, resulting in material damage, performance deterioration.

(2) Analyzed from the macroscopic point of view of the coal body, there are natural defects inside the coal body during the development process, such as fissures and joints, etc. The action of machinery in the process of mining, transportation and processing will cause damage to the internal structure of the coal body itself. The condition of impact experiment is under the action of triaxial pressure, the axial pressure acts on the specimen, and the fissures inside the specimen are closed under the action of pressure, thus increasing the denseness of the coal increasing the strength of the coal, i.e., the pressure-dense effect, and the action of stress wave under the action of multiple impacts leads to the development of fissures in the coal body and the deterioration of performance.

The peak stress of group 4 four specimens showed an increasing trend with the increase of the number of impacts. The reason for the analysis is that the randomness of coal fracture distribution and the inhomogeneity of structure distribution lead to the difference of macroscopic mechanical properties between the group 4 specimens and the first 3 groups, and there may be more cracks in the group 4 specimens. As seen from the basic parameters of the specimens in subsection 2.3.2, the results of ultrasonic wave velocity tests for specimens XH-4, XH-8 and XH-12 were 1.78 km/s, 1.97 km/s and 1.88 km/s, respectively, and the results of ultrasonic wave velocity tests for specimen XH-16 were 1.56 km/s; the results of mass tests for specimens XH-4, XH-8 and XH-12 were The results of ultrasonic wave velocity test and mass test of specimen XH-16 are smaller than those of specimen XH-4, XH-8 and XH-12, which are 140.361g, 136.591g and 139.298g, respectively, and the result of mass test of specimen XH-16 is 134.812g. It can be seen that with a small difference in volume, the results of ultrasonic wave velocity test and mass test of specimen XH-16 are smaller, so there are relatively more macroscopic cracks inside the specimen, which can withstand more pressure-density effect. Therefore, the strength of specimen XH-16 increases gradually with the increase of the number of damage impact.



### 3.3.2 The relationship between the peak stress and damage impact times

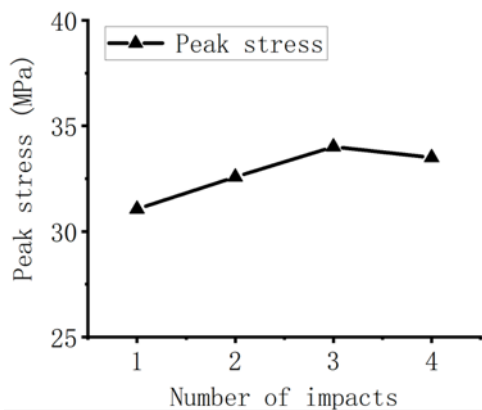
The relationship between the peak stress and the number of damage impacts for the four groups of specimens is shown in Figure 3.2. The peak stresses of the specimens increased with the number of damage impacts due to the compression-density effect and the closure of microscopic cracks, and began to decrease at the end of the compression-density stage, showing the expansion of macroscopic cracks and the deterioration of mechanical properties of the specimens. According to the one-dimensional stress wave theory, when the stress wave propagates in two different materials, the following relationship exists.

$$F = \frac{\rho_2 c_2 - \rho_1 c_1}{\rho_2 c_2 + \rho_1 c_1}, -1 < F < 0 \quad (3.18)$$

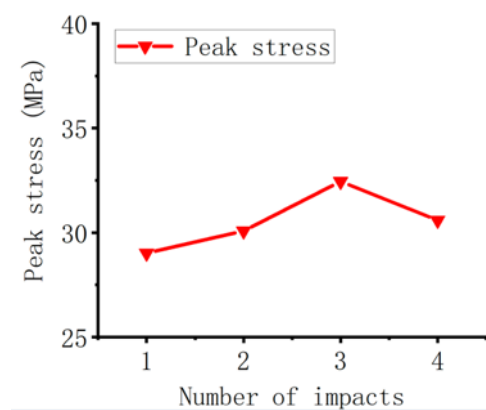
$$\sigma'_t(t) = (1+F)\sigma_i(t) \quad (3.19)$$

$$\sigma_i(t) = (1+F)(1-F)\sigma_i(t) \quad (3.20)$$

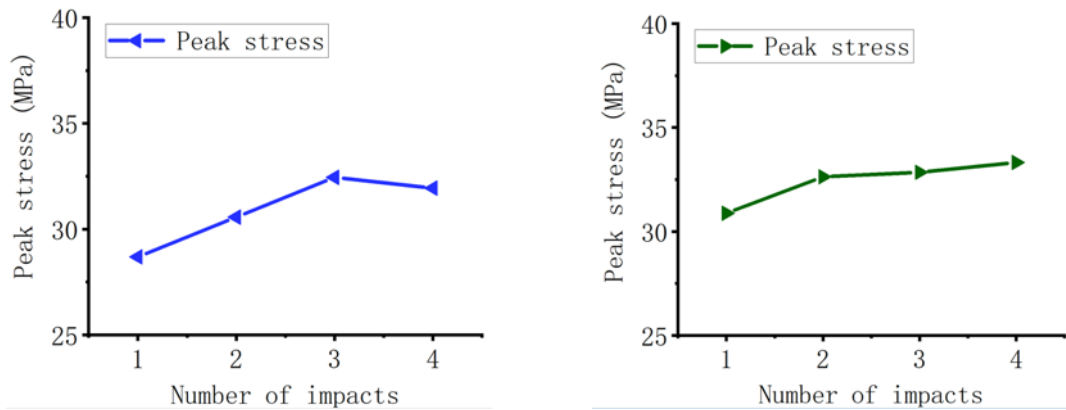
Where  $\rho_1 c_1$  is the magnitude of the wave impedance of the rod,  $\rho_2 c_2$  is the magnitude of the wave impedance of the specimen, F denotes the reflection coefficient of the stress wave in two different materials,  $\sigma'_t$  is the transmitted wave of the material, and  $\sigma_i$  is the transmitted wave of the rod.



(a) Peak stress of 4-cycle impact damage evolution of XH-4



(b) Peak stress of 4-cycle impact damage evolution of XH-8



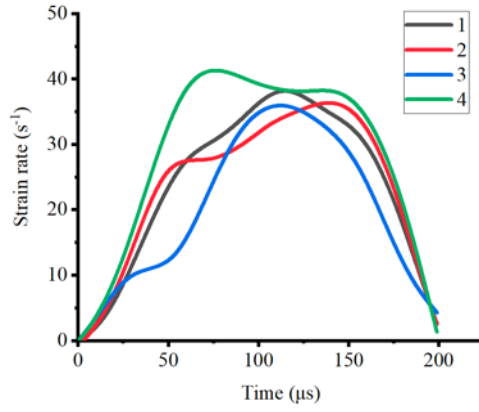
(c) Peak stress of 4-cycle impact damage evolution of XH-12      (d) Peak stress of 4-cycle impact damage evolution of XH-16

**Fig. 3.2 Relationship between damage evolution peak stress and damage impact times**

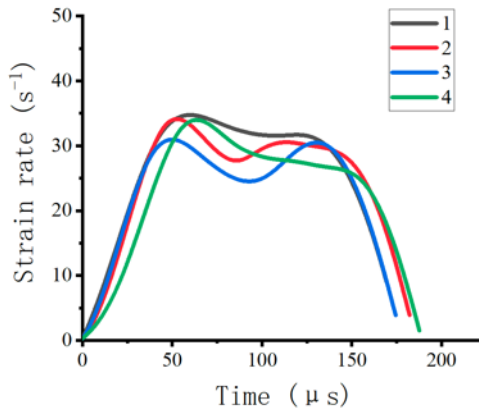
At the end of the compression and density stage, with the increase of the number of damage impacts, the damage inside the specimen will continue to expand, and the impedance of the corresponding coal body to the stress wave will continue to decrease, which will cause the reflection coefficient  $F$  of the stress wave to decrease, according to Equation (3.20), and through Equation (3.22) and (3.23), if we ignore the multiple reflections and transmissions of the stress wave in the material, the experimental design for equal-amplitude cyclic impact, so the amplitude of the incident wave is constant, the transmitted wave will keep getting smaller, so at the end of the compressional density stage, with the increase in the number of damage impact, the peak stress suffered by the coal specimen will keep getting smaller.

### 3.3.3 Relationship between the average strain rate and the number of damage impacts

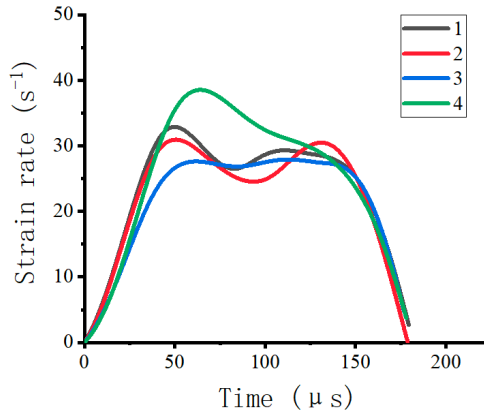
The time course curves of strain rate for the four groups of specimens are shown in Figure 3.3. The time course curves of strain rate of damage evolution for each group of specimens after four cycles of impact are basically the same, and it can be seen that when the specimens are loaded with impact air pressure of 0.2 MPa, the maximum strain rate of specimens XH-4, XH-8 and XH-12 shows a decrease and then increase with the increase of the number of damage impacts, and the maximum strain rate of specimens XH-16 keeps decreasing with the increase of the number of damage impacts. The maximum strain rate of specimen XH-16 decreased with the increase of the number of damage impacts, and the regular change was consistent with the stress-strain curve of the specimen.



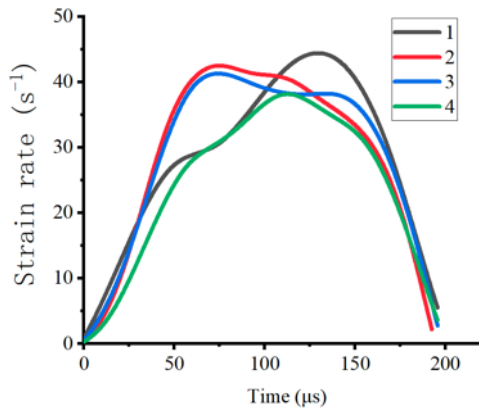
(a) Time course graph of 4-cycle impact strain rate of XH-4



(b) Time course graph of 4-cycle impact strain rate of XH-8

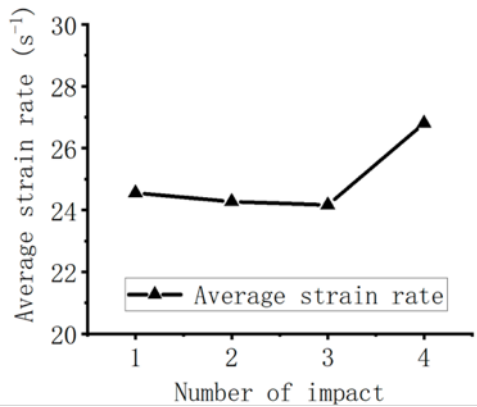


(c) Time course graph of 4-cycle impact strain rate of XH-12

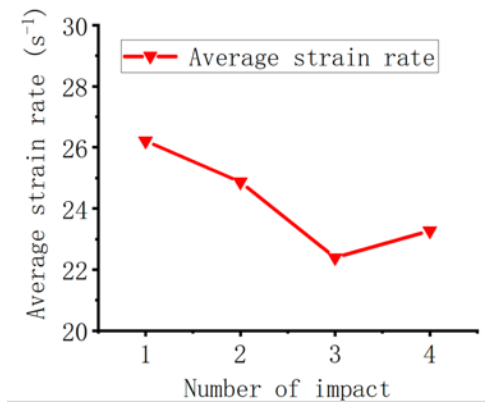


(d) Time course graph of 4-cycle impact strain rate of XH-16

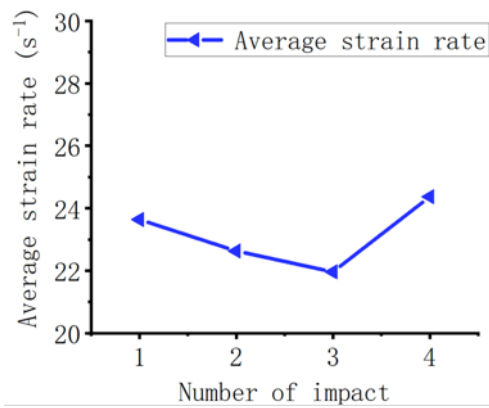
Fig. 3.3 Strain rate time history curve of specimen damage evolution



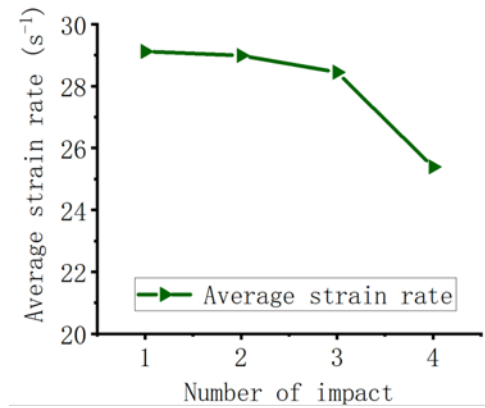
(a) Average strain rate of 4-cycle impact damage evolution of XH-4



(b) Average strain rate of 4-cycle impact damage evolution of XH-8



(c) Average strain rate of 4-cycle impact damage evolution of XH-12



(d) Average strain rate of 4-cycle impact damage evolution of XH-16

Fig. 3.4 relationship between average strain rate and damage impact times

The average strain rates for four cycles of loading were calculated to be  $24.55\text{s}^{-1}$ ,  $24.27\text{s}^{-1}$ ,  $24.16\text{s}^{-1}$  and  $26.8\text{s}^{-1}$  for specimen XH-4;  $26.21\text{s}^{-1}$ ,  $24.87\text{s}^{-1}$ ,  $22.39\text{s}^{-1}$  and  $23.27\text{s}^{-1}$  for specimen XH-8;  $23.64\text{s}^{-1}$ ,  $22.63\text{s}^{-1}$ ,  $21.96\text{s}^{-1}$  and  $24.37\text{s}^{-1}$  for specimen XH-12; and  $29.12\text{s}^{-1}$ ,  $28.99\text{s}^{-1}$ ,  $28.45\text{s}^{-1}$  and  $25.37\text{s}^{-1}$  for specimen XH-16. Figure 3.4 shows the variation of the average strain rate of the four groups of specimens versus the number of impacts, and it can be seen that the average strain rate of the specimen changes with the increase of the number of impacts with a certain pattern. The average strain rate of the specimens represents the deformation capacity of the specimens. The average strain rates of specimens XH-4, XH-8 and XH-12 show the law of decreasing and then increasing with the increase of the number of impact damage by cumulative damage; the average strain rate of specimen XH-16

gradually decreases with the increase of the number of impacts. The reason for the analysis is the same as that for the gradual increase of peak stress, which is due to the existence of macroscopic and microscopic cracks in the specimen, and the compression-density effect of the specimen under the action of stress wave and triaxial circumferential pressure, resulting in the increasing wave impedance of the specimen at the early impact damage. When the compression-density phase of the specimen ends, the average strain rate of the specimen begins to increase, which is due to the effect of impact damage damage evolution to reduce the wave impedance capacity of the specimen, resulting in the reflection coefficient  $F$  of the stress wave of the specimen decreasing, and its absolute value gradually increases because the reflection coefficient  $F$  of the stress wave is negative. Through the formula (3.21), it is known that the absolute value of the reflection coefficient  $F$  of the stress wave increases, and the corresponding strain rate also increases, and the elastic deformation capacity of the specimen gradually decreases, and the plastic deformation stage begins to gradually produce macroscopic cracks, so the average strain rate of the specimen increases.

---

### 3.3.4 Triaxial Surrounding Pressure Damage Evolution Law of Coal

From the perspective of the difficulty of the parameter measurement as well as the experimental conditions of the two perspectives, the macroscopic perspective of which the change in the elastic modulus of the specimen is selected to calculate the damage degree of the specimen, that is, the formula introduced in section 3.2.1 (3.7)  $D = 1 - E_n/E_0$  to calculate, where  $E_n$  is the elastic modulus of the specimen after the  $n$ th test,  $E_1$  is the elastic modulus of the specimen after the first impact.

From the stress-strain curves of the four groups of damage evolution specimens and the strain rate time course curves, it can be seen that after four cycles of impact damage, the specimens did not break and all showed good elastic deformation before the peak stress, and the method of  $E_q$ . (3.24) was used in this paper to calculate the elastic modulus of the specimens <sup>[59]</sup>.

$$E = \frac{\sigma_2 - \sigma_1}{\varepsilon_2 - \varepsilon_1} \quad (3.21)$$

Where  $\sigma_2$  and  $\sigma_1$  represent the stress magnitude at 60% and 40% of the peak stress-strain curve, respectively, and  $\epsilon_2$  and  $\epsilon_1$  represent the strain magnitude at 60% and 40% of the peak stress-strain curve, respectively.

According to the peak stress of the damage evolution impact damage of each specimen, the corresponding 60% and 40% stresses and strains were identified on the stress-strain curve graph, and the elastic modulus of the four groups of specimens after each impact was calculated by equation (3.24), and the specific data are shown in Table 3.1. The stress-strain curve of the 3rd damage impact of specimen XH-12 was selected as a typical example, and the two points corresponding to 60% and 40% of the peak of the stress-strain curve are shown in Figure 3.5.

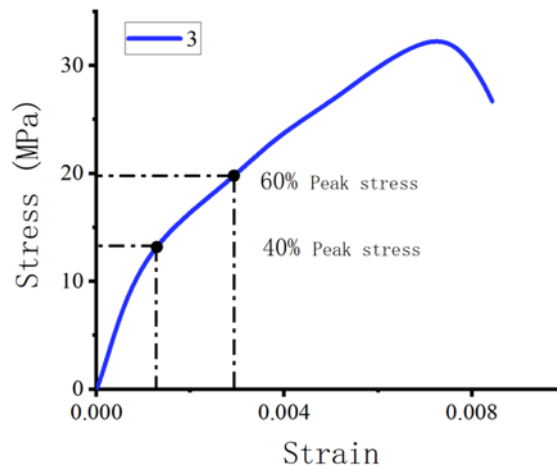
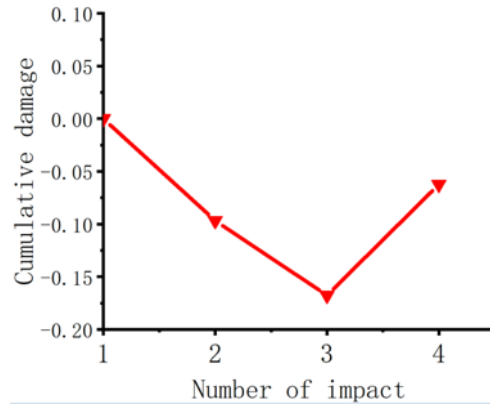
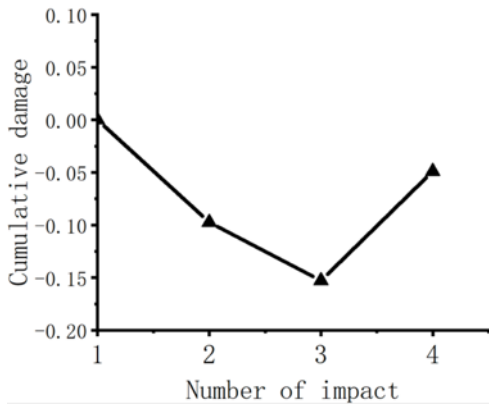


**Table 3.1 Relevant values for calculating elastic modulus**

	Impact times	Peak stress /MPa	60% stress/M Pa	60% strain	40% stress/M Pa	40% strain	E/MPa
XH-4	1	31.06	18.63	0.00376	12.43	0.00256	5167
	2	32.28	19.55	0.0035	13.03	0.00235	5670
	3	34.01	20.4	0.00321	13.61	0.00207	5956
	4	33.5	20.12	0.00212	13.4	0.00088	5419
XH-8	1	29.02	17.41	0.00252	11.61	0.00132	4833
	2	30.08	18.05	0.00304	12.06	0.00191	5301
	3	32.45	19.47	0.0018	12.98	0.00065	5643
	4	30.59	18.357	0.00321	12.247	0.00202	5134

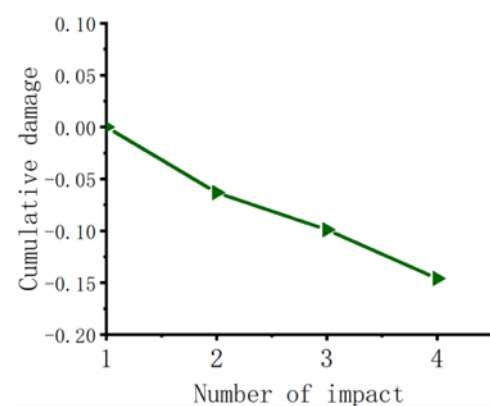
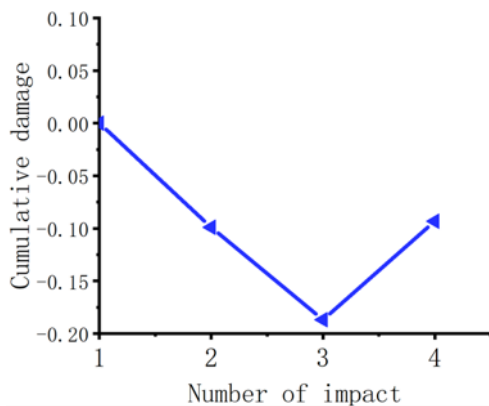
<b>XH-12</b>	<b>1</b>	<b>28.69</b>	<b>17.22</b>	<b>0.00322</b>	<b>11.48</b>	<b>0.00158</b>	<b>3500</b>
	<b>2</b>	<b>30.57</b>	<b>18.34</b>	<b>0.0033</b>	<b>12.224</b>	<b>0.00171</b>	<b>3847</b>
	<b>3</b>	<b>32.45</b>	<b>19.47</b>	<b>0.00284</b>	<b>12.99</b>	<b>0.00128</b>	<b>4154</b>
	<b>4</b>	<b>31.94</b>	<b>19.17</b>	<b>0.00313</b>	<b>12.78</b>	<b>0.00146</b>	<b>3826</b>
<b>XH-16</b>	<b>1</b>	<b>30.88</b>	<b>18.53</b>	<b>0.00295</b>	<b>12.35</b>	<b>0.00142</b>	<b>4039</b>
	<b>2</b>	<b>32.63</b>	<b>19.578</b>	<b>0.00296</b>	<b>13.059</b>	<b>0.00144</b>	<b>4294</b>
	<b>3</b>	<b>32.85</b>	<b>19.73</b>	<b>0.00222</b>	<b>13.16</b>	<b>0.00074</b>	<b>4439</b>
	<b>4</b>	<b>33.32</b>	<b>19.99</b>	<b>0.0032</b>	<b>13.325</b>	<b>0.00176</b>	<b>4628</b>

After obtaining the elastic modulus of the specimens after each impact, the damage degree of the specimens after each impact was calculated according to the formula  $D=1-E_n/E_0$ . The value of D was greater than 0 that the specimens produced positive damage, and the value of D was less than 0 that the specimens experienced negative damage. Each group of specimens was subjected to four damage impacts, which corresponded to four values of the elastic modulus, and three degrees of damage could be calculated using the elastic modulus of the specimen after the first impact as the reference. Expressed as a percentage, the damage degree of specimen XH-4 after the 2nd impact was calculated to be -9.73%, the damage degree after the 3rd impact was -5.05%, and the damage degree after the 4th impact was 9.01%, and the damage degree after each damage impact of the specimen was accumulated to calculate the cumulative damage of each group of specimens after 4 impacts, and the cumulative damage of specimen XH-4 was -5.77%; specimen XH-8 in the second impact after the degree of damage is -9.67%, the third is -6.46%, the fourth is 9.02%, the cumulative damage is -7.11%; specimen XH-12 in the second impact after the degree of damage is -9.90%, the third is -7.99%, the fourth is 7.88%, the cumulative damage is -10.01%; the damage of specimen XH-16 after the 2nd impact was -6.32%, the 3rd was -3.37%, the 4th was -4.26%, and the cumulative damage was -13.95%. The relationship between the number of damage impacts and cumulative damage of the specimen is shown in Figure 3.6.



(a) Cumulative damage of specimen XH-4

(b) Cumulative damage of specimen XH-8



(c) Cumulative damage of specimen XH-12

(d) Cumulative damage of specimen XH-16

**Fig. 3.6 Relationship between cumulative damage and impact times**

As shown in Figure 3.6, after four sets of specimens were subjected to four cyclic loading damage evolution impacts, the accumulated damage of the specimens were all negative, and the first three impacts of specimens XH-4, XH-8 and XH-12 were negative damage. This is the result of the pressure-density effect, the fourth impact of the damage degree becomes a positive value. It indicates that the impact air pressure of certain size can increase the denseness of the coal body and make the pores and fissures inside the coal body compressed and closed to improve its bearing capacity. However, with the increasing number of impacts, the speed of coal body compacting cannot catch up with the damage caused by stress, the structure of coal body changes, the bearing capacity becomes weaker, and the accumulated damage increases, which eventually leads to rupture. The accumulated damage of group 4 specimens were all negative for the reasons as described in peak stress and average strain rate. The result of ultrasonic wave velocity test of specimen XH-16 is 1.56km/s and the result of mass test is 134.812g. Compared with other



specimens, the results of ultrasonic wave velocity test and mass test of specimen XH-16 are smaller in the case of small volume difference, so there are relatively more macroscopic cracks inside the specimen, which can bear more compression-density action. The compression-density phase of the specimen dominates the four damage impacts, so all four damages are negative. If you want to achieve a more pronounced effect of damage evolution of triaxially enclosed compressed coal, the number of cyclic loading impact damage should be increased appropriately.

---

### **3.4 Summary of the chapter**

This chapter focuses on the analysis and study of the damage evolution characteristics of coal cyclically loaded impact damage under triaxial pressure conditions. The selection of damage factors, including the definition and calculation of damage factors, the description of strain equivalence assumptions and the interpretation of damage evolution are introduced before the analytical work is carried out. By analyzing the stress-strain curves, the relationship between peak stress and number of impacts, and the relationship between average strain rate and number of impacts for four groups of cyclically loaded impact damaged specimens, and by solving the elastic modulus of the specimens after each impact damage, the damage degree of the specimens after each impact was calculated, and finally the cumulative damage law of triaxial pressure coal after cyclic impact was determined. The main conclusions drawn are:

(1) The stress-strain curves of the specimens for the four damage impacts showed the same trend. Each stress-strain curve showed a certain degree of rebound after reaching the peak stress, indicating that the specimens did not experience macroscopic damage after the four damage impacts, and the rebound was due to the elastic energy released from the specimens during stress unloading.

(2) With the increase of the number of damage impacts, the peak stress and elastic modulus of the specimens showed a trend of first increasing and then decreasing, and the average strain was first decreasing and then increasing. Analysis due to the compression-density effect and the microscopic fracture closure effect, so that the specimen in the early stage of the damage impact on the impedance of the stress wave increased, so the peak stress, elastic modulus increased, at the end of the compression-density stage, the peak stress of the specimen began to decrease,

showing the expansion of macroscopic cracks in the specimen, the deterioration of mechanical properties.

(3) The specimens that experienced four damage impacts had negative cumulative damage values, which were -5.77%, -7.11%, -10.01% and -13.95% for the four groups of specimens, respectively.

In the study of this chapter, the law of cyclic impact damage evolution of 4 groups of coal bodies was mainly analyzed, and some preliminary research results were obtained, but some depth and improvement are needed, for example, in the future research of coal damage evolution, the number of cyclic impact damage can be appropriately increased in order to achieve the effect of cyclic impact coal damage.

## **4 Analysis of dynamic impact failure characteristics of triaxial confining coal**

---

### **4.1 Introduction**

---

The design concept of the SHPB impact damage experiment was to divide 16 specimens into 4 groups, and the variable between the 4 groups was the strength of the last crushing impact. The variable within each group is the number of damage impact damage, and there is another group of specimens with a single crushing impact under triaxial pressure as a "zero" damage control group. The first aspect is the study of the relationship between the damage evolution of the specimens under triaxial pressure and the number of damage impacts, which is summarized in Chapter 3. The second aspect is to analyze the mechanical properties of dynamic impact damage of specimens with different damage levels under triaxial pressure conditions, and finally to analyze the dynamic mechanical properties of specimens with different impact velocities under triaxial pressure conditions.

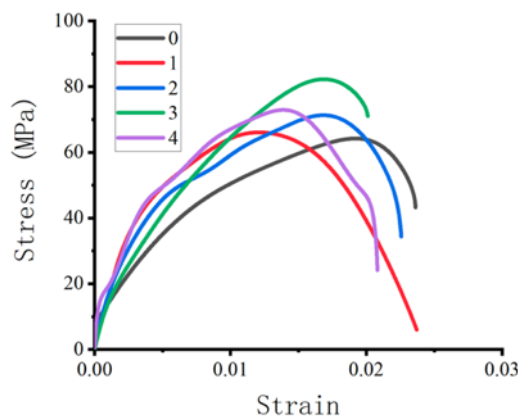
In this chapter, the remaining two aspects of the study are systematically analyzed in conjunction with the findings of the damage evolution of the specimens studied in Chapter 3. The stress-strain curve variation law, strength variation law and crushing morphology of the specimens under different loading conditions are analyzed, and the results of the study provide references for the study of dynamic impact damage mechanism of coal bodies, and also provide a reference basis for the early warning as well as prevention and control of coal rock dynamic hazards.

### **4.2 Mechanical properties analysis of dynamic load impact damage of damaged coal under triaxial pressure conditions**

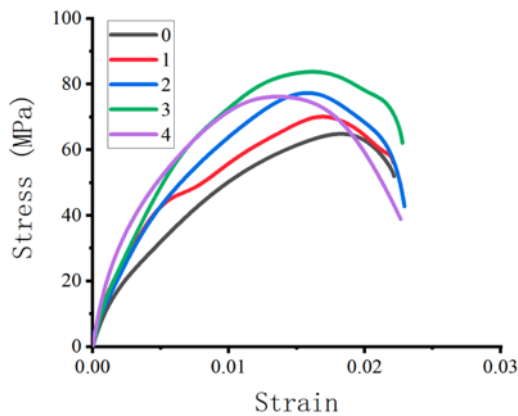
---

The last impact damage of the specimens (0.8 MPa, 1.0 MPa, 1.2 MPa and 1.4 MPa air pressure impact damage) was the crushing impact. Figure 4.1 shows the crushing impact stress-strain curves of specimens with different damage impact times under triaxial envelope pressure conditions, and each group of curves shows a good regularity, and the overall trend changes are relatively similar. At first, each curve shows a period close to a straight line, and then the slope of the tangent line of the curve gradually decreases and the curve is "up-convex". With the propagation

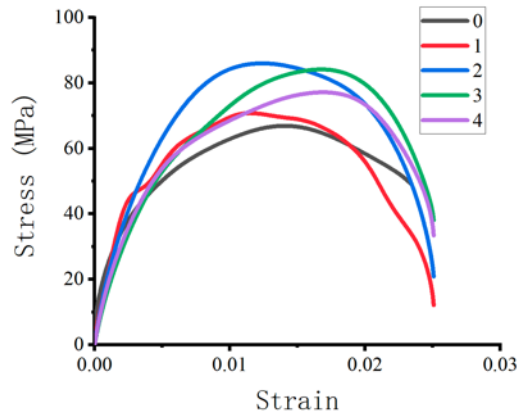
of the stress wave, the slope of the curve decreases to a greater extent, at this time the specimen under the action of dynamic load began to produce new cracks inside, the original cracks are also under the action of stress expansion, this stage for the plastic deformation of the material stage. The dynamic stress will appear a short plastic plateau near the peak, at this stage the stress remains the same with the increase of strain, the cracks inside the specimen continue to evolve and expand, the elastic modulus decreases rapidly, and the specimen starts to produce irreversible plastic deformation inside. After reaching the peak stress, the slope of the curve becomes negative, and the dynamic stress starts to decrease gradually, which can be considered as the plastic rebound stage of the material. After reaching the maximum value, the strain begins to decrease gradually. The larger the strain recovery value is, the better the elasticity of the material. In the stress-strain curve, the strain recovery value in the rebound stage is very small or no recovery, which indicates that the specimen has undergone more plastic deformation or has broken under the effect of crushing impact.



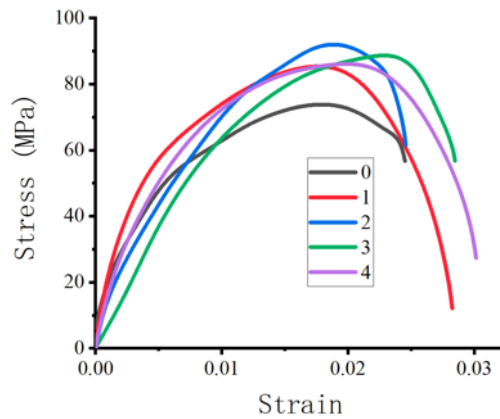
**(a) Stress-strain curve of 0.8 MPa impact air pressure specimen**



**(b) Stress-strain curve of 1.0 MPa impact air pressure specimen**



(c) Stress-strain curve of 1.2 MPa impact air pressure specimen



(d) Stress-strain curve of 1.4 MPa impact air pressure specimen

**Fig. 4.1 Crushing impact stress-strain curves of specimens with different degrees of damage**

Figure 4.1(a) shows the stress-strain curves of the 0.8 MPa air pressure crushing impact specimens, corresponding to GS-4, XH-1 - XH-4. With the increase of the number of damage impact damage, the peak magnitude of stress reached by the specimens increases and then decreases, respectively, to 64.21 MPa, 66.07 MPa, 71.27 MPa, 82.24 MPa and 72.90 The peak stresses of the specimens that experienced damage were larger than those of the undamaged specimens, and the pattern was consistent with the analysis in Chapter 3. This indicates that the compression-density phase of the specimen dominates in the early stage of cumulative damage, and the cumulative effect of cyclic impacts can make the coal body denser and increase the load-bearing capacity in the compression-density phase. There are macroscopic and microscopic fractures inside the coal body, and under the action of triaxial circumferential pressure and 0.2 MPa damage impact, the coal body will go through the compacting phase to increase its own bearing capacity. When the compacting stage is over, the internal structure of the coal body will be gradually destroyed as the damage impact continues, and the more the

number of damage impact, the more serious the damage of the coal body structure and the more obvious the decrease of the bearing capacity.

Figure 4.1(b) shows the stress-strain curves of the 1.0 MPa air pressure crushing impact specimens, corresponding to GS-3, XH-5 - XH-8. With the increase of the number of damage impact damage, the peak stresses that the specimens can reach first increase and then decrease, respectively, 64.85 MPa, 70.09 MPa, 77.06 MPa, 83.62 MPa and 76.09 MPa. The curve variation pattern is the same as that of group 1, and the peak stress reached by the damage impacted specimens is greater than that of the specimens that have not experienced the damage impact, indicating that the coal body also experienced the compression-density stage before it gradually started to produce damage. Figure 4.1(c) shows the stress-strain curves of the 1.2 MPa air pressure crushing impact specimens, corresponding to GS-2, XH-9 - XH-12. The peak stresses show a trend of increasing and then decreasing with the increase of impact times, and the peak stresses are 66.91 MPa, 70.79 MPa, 86.00 MPa, 84.16 MPa and 77.15 MPa. The stress peaks of the specimens that had not experienced damage impact were also the smallest. Figure 4.1(d) shows the stress-strain curves of the 1.4 MPa air pressure crushing impact specimens, corresponding to GS-1, XH-13 - XH-16. The peak stresses of the specimens also increased and then decreased with the number of impacts, with magnitudes of 73.81 MPa, 85.36 MPa, 91.96 MPa, 88.67 MPa, and 86.07 MPa, respectively. The peak stress of the specimens that had not experienced damage strikes was likewise the smallest among the five groups of 1.4 MPa crushing impact specimens. the analysis of the stress-strain curves of the four groups of specimens illustrates that the specimens become stronger in the initial stage of cyclically loaded damage impacts on the coal body under triaxial peritectic pressure conditions due to the pressure-dense effect of bearing capacity.

Figure 4.2 shows a graph of the damage crushing results of the specimen after impact damage. The variable in each column is the number of damage impacts, and the variable in each row is the magnitude of the crushing impact air pressure. The crushing pattern of the specimen is consistent with the pattern of stress-strain curve analysis. Initially, under the joint action of damage impact and triaxial circumferential pressure conditions, the specimen will go through a compression-dense stage, and as the number of damage impacts increases, the specimen becomes dense and the

load-bearing capacity increases. As shown in Figure 4.2, the number of damage impacts of the specimens increases from left to right. Under the same crushing impact, the specimens that have not undergone damage impacts have the most severe crushing, followed by the specimens that have experienced only one damage impact, the specimens that have undergone two damage impacts have less crushing than the specimens that have undergone one damage impact, and the specimens that have undergone three and four damage impacts have little overall difference in crushing. The results of the crushing pattern of the specimens corresponded to the pattern of stress-strain curve analysis of the specimens.

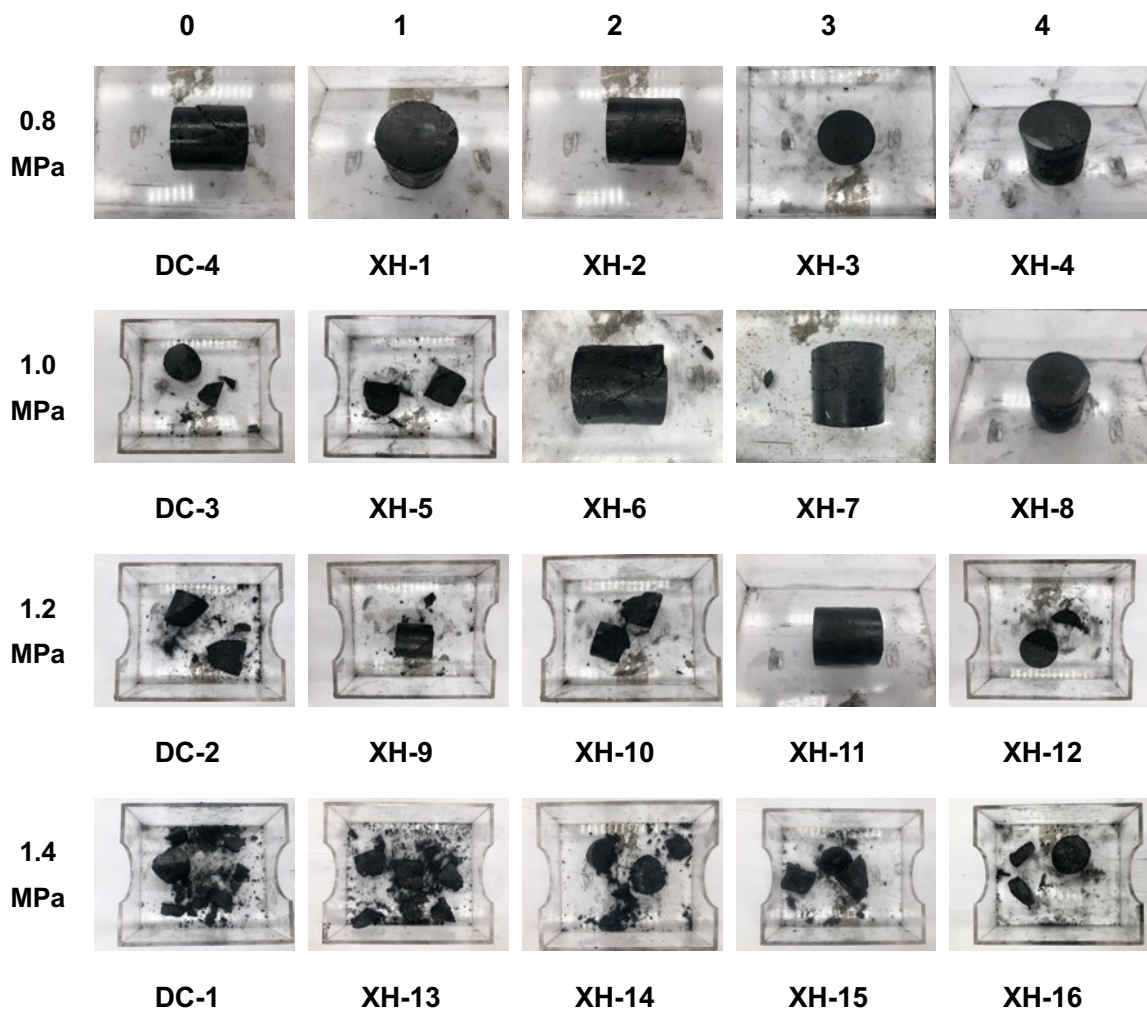
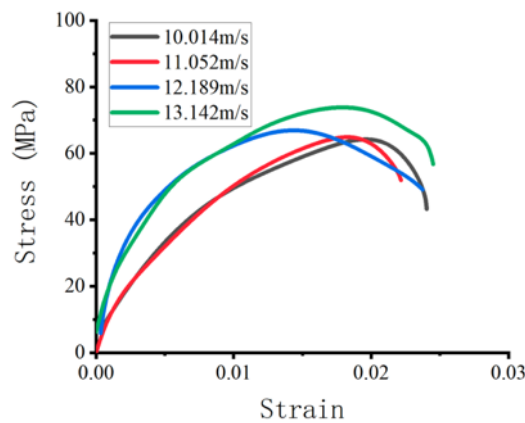


Fig. 4.2 Results of sample damage and breakage

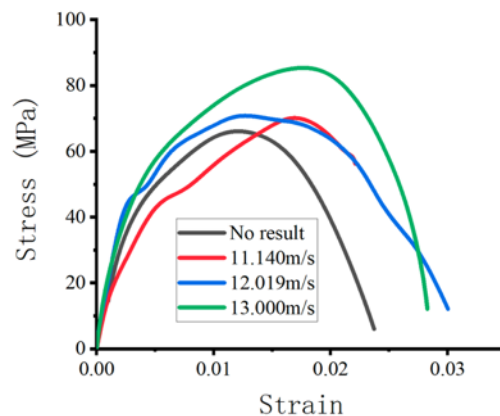
### 4.3 Dynamic mechanical characterization of coal with different impact velocities under triaxial pressure

#### 4.3.1 Analysis of the stress-strain curve of coal at different impact velocities

The impact velocity of crushing impact is used as the variable, and the circumferential pressure condition is fixed to 10 MPa for axial pressure and 15 MPa for radial circumferential pressure, to study the dynamic mechanical characteristics of the coal samples with the same damage impact number at different impact velocities under triaxial circumferential pressure conditions. Figure 4.3 shows the stress-strain curves of the same damage impact number specimens under different impact velocities (air pressure), and the velocities in the annotated boxes are the bullet velocities corresponding to 0.8 MPa, 1.0 MPa, 1.2 MPa and 1.4 MPa crushing impact air pressure.

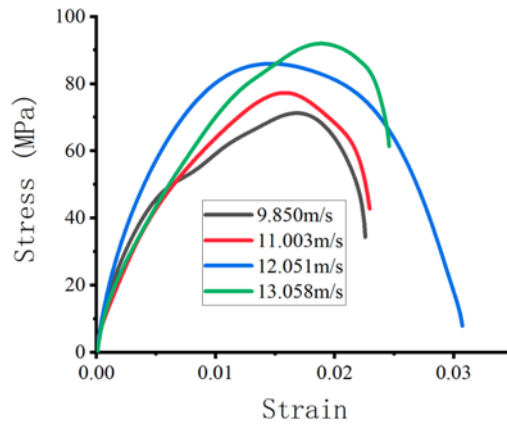


(a) Stress-strain curves of non-damaging impact with different impact velocities

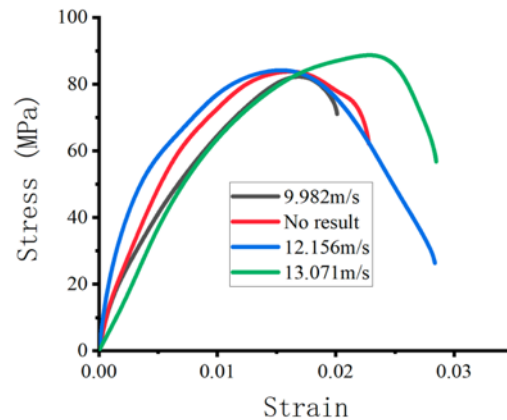


(b) Stress-strain curves of one-damaging impact with different impact velocities

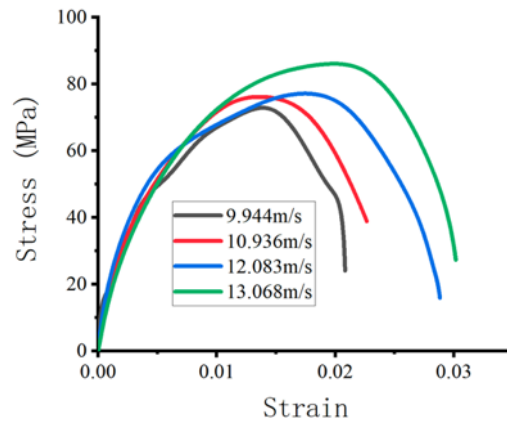




(c) Stress-strain curves of two-damaging impact with different impact velocities



(d) Stress-strain curves of three-damaging impact with different impact velocities



(e) Stress-strain curves of four-damaging impact with different impact velocities

**Fig. 4.3 Stress-strain curves of different impact velocities specimens**

Figure 4.3 (a) shows the stress-strain curves for different crushing impact velocities under undamaged impact conditions, and the peak stresses corresponding to crushing impact are 64.21 MPa, 64.85 MPa, 66.91 MPa, and 73.81 MPa, respectively; Figure 4.3 (b) shows the stress-strain curves for different crushing impact velocities of the specimens after 1 damage impact, and the peak stresses of each curve are 66.07MPa, 70.09MPa, 70.79MPa and 85.36MPa; Figure 4.3 (c) The impact velocities of the specimens are 9.850m/s, 11.003m/s, 12.051m/s and

13.058m/s respectively, and the corresponding stress peaks are 71.27MPa, 77.06MPa, 86.00MPa and The stress peaks corresponding to the lines in Figure 4.3(d) are 82.24, 83.62, 84.16 and 88.67 MPa, respectively; Figure 4.3(e) shows the stress-strain curves of the specimens undergoing four damage impacts with different impact velocities, the crushing impact velocities of each specimen are 9.944, 10.936, 12.083 and 13.068 m/s, and the corresponding peak stresses were 72.90 MPa, 76.09 MPa, 77.15 MPa, and 86.07 MPa.

The overall stress-strain curves of the specimens with different crushing impact speeds have a certain regularity. The stress peak increases with the increase of the crushing impact speed, and there is a more obvious plastic plateau in each stress-strain curve. This indicates that the specimens were deformed or broken, and the larger the impact velocity, the longer the plastic plateau of the curve lasts, and the more serious the damage or broken specimens are. In the rebound stage of each curve strain rebound value is small or no rebound, indicating that the specimen is severely damaged or even broken under the action of crushing impact. As shown in Figure 4.2, the crushing results of specimen damage are shown in each column of the graph, where the variable is the magnitude of the air pressure of the crushing impact. Specimen crushing results in line with the law of stress-strain curve analysis, from the figure can be seen, in the case of the same damage impact in the three axes of the circumferential pressure, the greater the crushing impact air pressure, that is, the greater the impact velocity, the more serious the degree of damage to the broken specimen. The greater the impact velocity, the greater the crushing energy suffered by the specimen, the more serious the structural damage caused to the specimen, the more significant the crushing effect. Combined with the actual engineering practice, the mining and crushing efficiency of coal and rock can be improved by increasing the impact velocity.

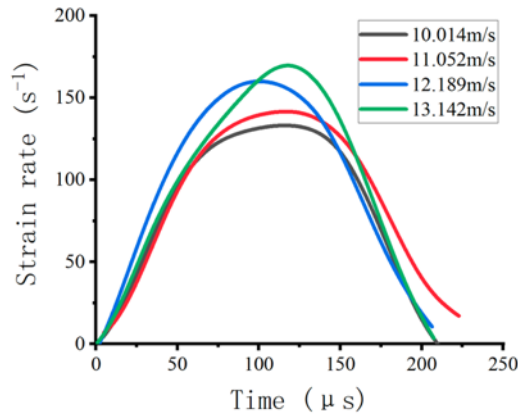
---

#### **4.3.2 Time course analysis of strain rate curve of coal under different impact velocities**

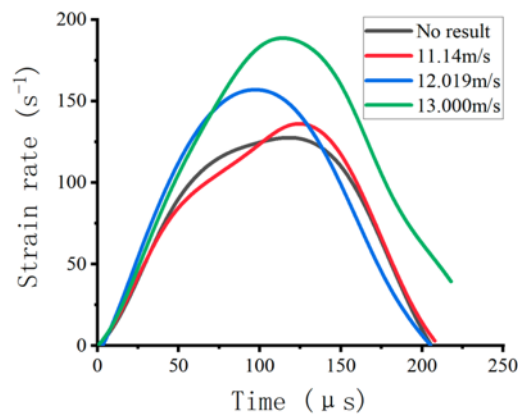
---

The time course curves of the strain rate of the specimen under different crushing impact velocities were calculated and plotted by combining the reflected wave voltage signals measured by the super dynamic digital acquisition instrument with the high frequency noise reduction processing and the corresponding equations as

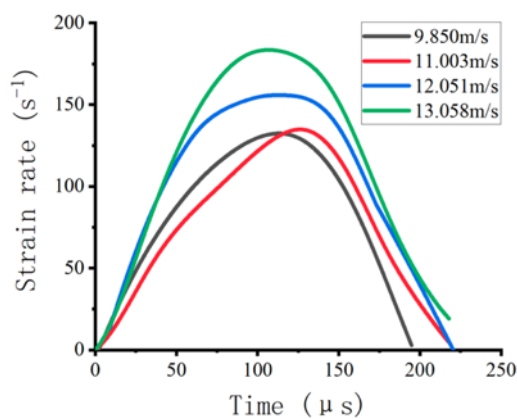
shown in Figure 4.4. The overall change trend of the five sets of curves was the same and could be divided into three stages. The slope of the tangent line of the curve becomes smaller until it reaches the peak, and finally the curve enters the accelerated decline phase, and the strain rate decreases rapidly.



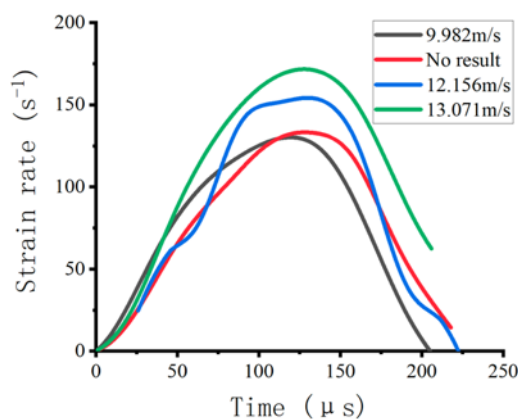
**(a) Non-damaging impact specimens**



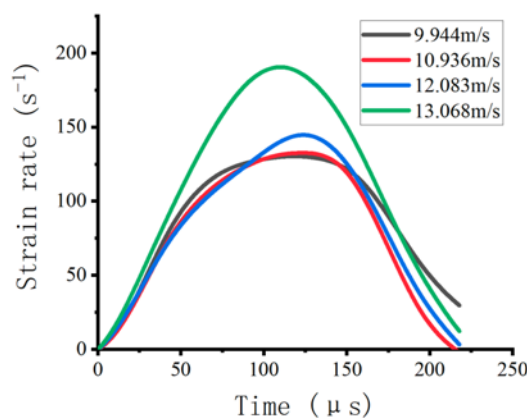
**(b) 1-damaging impact specimens**



**(c) 2-damaging impact specimens**



(d) 3-damaging impact specimens



(e) 4-damaging impact specimens

**Fig. 4.4 Strain rate time history curves of specimens with different impact velocities**

As seen in Figure 4.4, the higher the dynamic crushing impact velocity of the specimen, the higher the peak value of the strain rate it can reach. The reason for this analysis is due to the fact that at lower dynamic impact velocities, only a few cracks inside the specimen are involved in the damage process. Under the action of higher dynamic impact velocity, the original crack inside the specimen expands and evolves while new cracks are generated under the action of larger impact energy intensifying the damage to the coal body, which is manifested by the increase of the peak strain rate.

#### 4.4 Energy dissipation analysis of coal with different impact velocities under triaxial pressure

The stress wave energy produced by impacting the specimens at different impact speeds varies, causing different degrees of specimen fragmentation, and the effect of crushing impact at different impact speeds on the degree of specimen fragmentation is analyzed from the energy point of view [92].

The energies of the incident, reflected, and transmitted waves can be calculated from the time strain of the corresponding waves<sup>[93,94]</sup>, by the following equation:

$$E_I = A_0 \rho_0 C_0^3 \int_0^t \varepsilon_I^2(t_0) dt_0 \quad (4.1)$$

$$E_R = A_0 \rho_0 C_0^3 \int_0^t \varepsilon_R^2(t_0) dt_0 \quad (4.2)$$

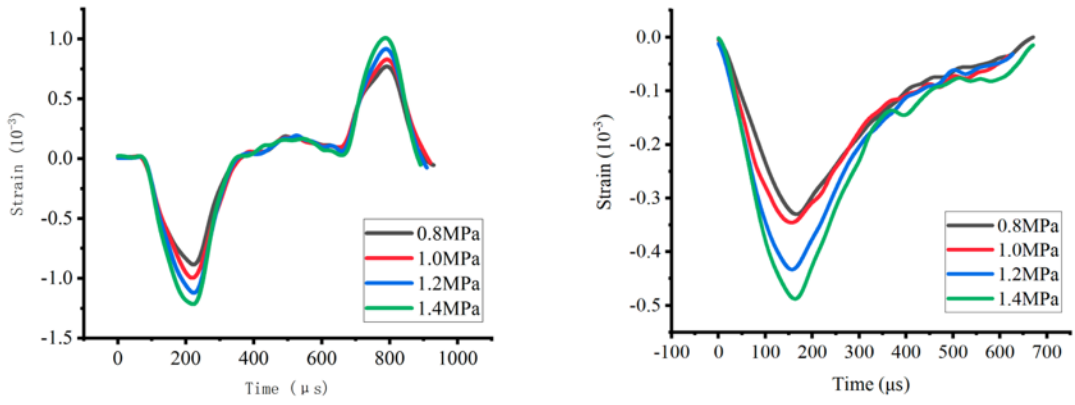
$$E_T = A_0 \rho_0 C_0^3 \int_0^t \varepsilon_T^2(t_0) dt_0 \quad (4.3)$$

Where  $E_I$  is the incident wave energy,  $E_R$  is the reflected wave energy and  $E_T$  is the transmitted wave energy;  $A_0$ ,  $\rho_0$  and  $C_0$  are the cross-sectional area, density and acoustic wave propagation velocity of the rod, respectively, and the cross-sectional area  $A_0$ , density  $\rho_0$  and acoustic wave propagation velocity  $C_0$  of the rod are  $0.196\text{m}^2$ ,  $7740\text{kg/m}^3$  and  $5159\text{m/s}$ , respectively;  $\varepsilon_I(t_0)$ ,  $\varepsilon_R(t_0)$  and  $\varepsilon_T(t_0)$  are the time strains of incidence, reflection and transmission, respectively.

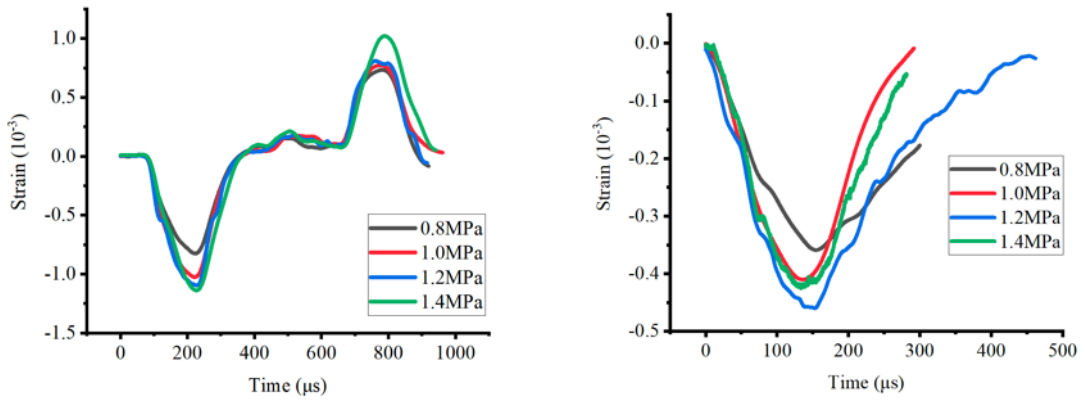
According to the law of conservation of energy, the energy consumed by the stress wave acting on the specimen,  $E_C$ , is equal to the difference between the energy of the incident wave and the energy of the reflected and transmitted waves, as shown in the expression in Equation (4.4):

$$E_C = E_I - E_R - E_T \quad (4.4)$$

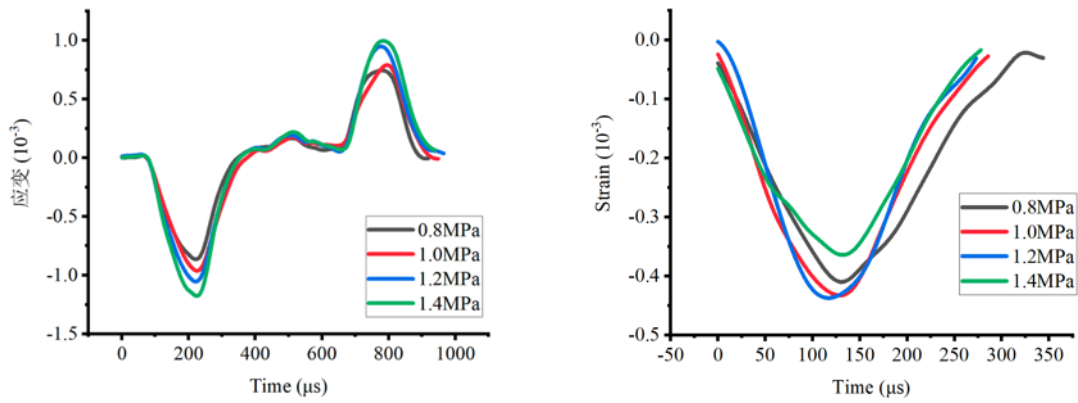
The time-voltage signal measured by the super dynamic data acquisition instrument was processed by high frequency noise reduction and combined with the corresponding calibrated K values of the rods to obtain the measured time-strain curves of the impact process. The incident wave strain, reflected wave strain and transmitted wave strain of coal samples with the same number of damage impacts at different crushing impact speeds are shown in Figure 4.5. Since the experimental setup could not control the equal impact velocity for each impact, the magnitude of impact velocity was expressed by different air pressure to achieve the equal incident wave amplitude.



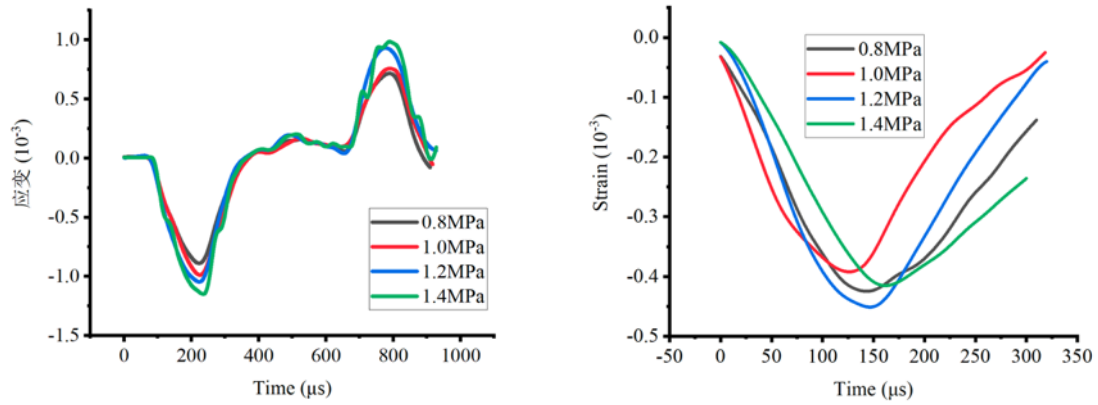
(a) Non-damaging impact specimens



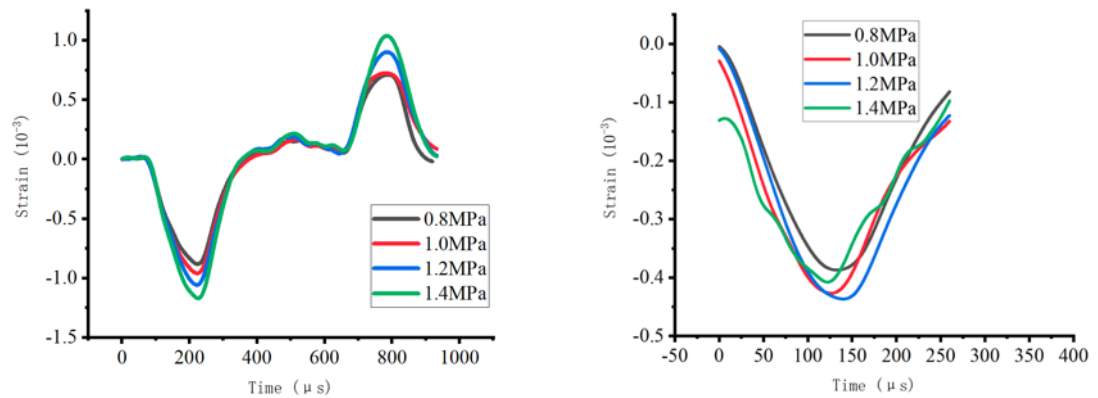
(b) 1-damaging impact specimens



(c) 2-damaging impact specimens



(d) 3-damaging impact specimens



(e) 4-damaging impact specimens

**Fig. 4.5 Time strain curves of specimens under different impact pressures**

According to equations (4.1)-(4.3), the incident, reflected and transmitted wave energies of each impact can be calculated by combining the corresponding rod data and time strain curves. According to Equation (4.4), the energy dissipated by damage or destruction of the specimen can be calculated. The specific calculation results are shown in Table 4.1.

**Table 4.1 Crushing impact energy results of specimens**

Damage impact times	Specimen number	Shock air pressure (MPa)	Incident energy (J)	Reflected energy (J)	Transmissive energy (J)	Dissipated energy (J)
0	DC-4	0.8	185	132	41	12
	DC-3	1.0	231	155	43	33
	DC-2	1.2	289	176	47	66
	DC-1	1.4	347	210	68	69
1	XH-1	0.8	164	123	34	7
	XH-5	1.0	245	161	39	45

	XH-9	1.2	285	184	49	52
	XH-13	1.4	328	220	53	55
2	XH-2	0.8	175	137	33	5
	XH-6	1.0	220	138	45	33
	XH-10	1.2	263	183	46	34
	XH-14	1.4	325	236	44	45
3	XH-3	0.8	185	113	56	16
	XH-7	1.0	227	132	59	36
	XH-11	1.2	263	186	40	37
	XH-15	1.4	308	213	56	39
4	XH-4	0.8	185	118	43	24
	XH-8	1.0	223	155	37	31
	XH-12	1.2	259	176	46	37
	XH-16	1.4	319	237	49	33

As seen in Table 4.1, under the same damage impact conditions, with the increase of the crushing impact air pressure, the energy of the incident wave increases, and the incident wave produces an average incident energy of 178.8 J, 229.2 J, 271.8 J and 325.4 J in order with the increase of the impact air pressure, and the corresponding reflected wave energy also increases; combined with the crushing results of the specimen, with the increase of the crushing impact air pressure, the The more obvious the degree of fragmentation of the specimen, the greater the energy consumed by the fragmentation.

#### 4.5 Summary of the chapter

In this chapter, dynamic impact damage experiments with variable damage times and variable impact velocities were carried out on 50 mm coal samples with length-to-diameter ratio of 1 using the SHPB triaxial pressure dynamic impact damage platform. The main discussions are: the change law of stress-strain mechanical properties of the specimens with different damage impact times under the same crushing impact, and the dynamic mechanical characteristics of the coal body under different damage conditions under triaxial pressure are obtained; the change law of stress-strain and strain rate of the coal under different dynamic impact velocities under triaxial pressure conditions are obtained. The main conclusions obtained are.

(1) Under the triaxial pressure conditions, the stress peak reached by the crushing impact stress-strain curve of the specimen increases and then decreases with the



increase of the number of damage impacts. The peak stress of specimens that have experienced damage impact is greater than the peak stress of specimens without damage impact. In the early stage of damage impact, the compression-density phase of the specimen dominates the impact process, and the low-energy impact can make the coal body become more dense and have an increased resistance to waves. As the impact continues the compression and density rate of the specimen and not on the rate of new crack development and expansion of the specimen, the specimen begins to produce structural damage, and the impedance capacity of the wave gradually becomes weaker.

(2) Under the triaxial pressure conditions, the degree of fragmentation of the specimens with different number of damage impacts was different. Under the same crushing impact, the crushing degree of the specimens without damage impact is the most serious, followed by the specimens with only one damage impact, the crushing degree of the specimens with two damage impacts is less than that of the specimens with one damage impact, and the overall difference between the crushing degree of the specimens with three and four damage impacts is not significant.

(3) Under the triaxial pressure condition, the coal body has strain rate effect. The higher the crushing impact velocity, the higher the stress peak that the specimen can reach, and the corresponding strain rate peak is also higher.

(4) Under the triaxial pressure condition, the coal body is broken at different impact velocities with different degrees. The greater the impact velocity, the greater the energy generated by the incident wave, the more serious the damage or fragmentation of the specimen, the smaller the block size of the specimen fragmentation, and the greater the energy consumed by the fragmentation.

## 6 Conclusions and outlooks

---

### 6.1 Conclusions

---

In this paper, 22 specimens with 60 impacts were selected by a combination of field experiments and data analysis to study the dynamic damage characteristics of triaxial pressure coal bodies under cyclic impact loading. The experimental design has three main parts: 1. SHPB dynamic impact damage experiment of cyclic impact triaxial pressure coal; 2. SHPB dynamic impact damage experiment of single impact triaxial pressure coal; 3. SHPB dynamic impact damage experiment of single-axis compression high-speed camera. The experimental settings of the surrounding pressure conditions are 10 MPa for axial pressure and 15 MPa for radial pressure. the purpose of the three sets of experiments is mainly to analyze and compare the damage damage patterns and dynamic mechanical properties of the coal body under the cyclic impact damage times and different impact damage speeds under triaxial pressure conditions. The high-frequency noise reduction process was performed on the collected raw voltage signals, and the stress-strain curves and strain rate time curves of the specimens after impact were plotted according to the experimental principle of SHPB. The change pattern of each curve and the damage fragmentation pattern of the specimen after impact are analyzed to study the damage evolution characteristics and dynamic impact damage mechanical properties of compressed coal under cyclic impact loading. The main contents and conclusive results of the full paper are:

(1) certain conditions of triaxial pressure can improve the bearing capacity of the specimen. Under the same damage impact pressure impact damage, the degree of fragmentation of the specimens without enclosing pressure is much higher than the degree of fragmentation of the specimens with enclosing pressure, the existence of enclosing pressure can significantly reduce the damage of the specimens.

(2) The peak stress and modulus of elasticity of the specimens with the increase of the number of damage impact showed a trend of first increasing and then decreasing, and the average strain rate showed a trend of first decreasing and then increasing. Analysis due to the compression of the fracture closure, the specimen in the early stage of the damage impact on the stress wave resistance is enhanced,

so the peak stress and elastic modulus with the increase in the number of damage impact increases, the average strain rate gradually decreases. When the damage impact reached a certain number of times, the specimen compression density speed and not on the specimen of new crack development and expansion, the specimen began to produce damage, load-bearing capacity gradually weakened, mechanical properties deteriorated, the wave impedance capacity decreased, showing a decrease in peak stress and elastic modulus, the average strain rate increased.

(3) The specimens that experienced four damage impacts had negative cumulative damage values, and the cumulative damage of the four groups of specimens was -0.0577, -0.0711, -0.1001 and -0.1395, respectively. the compression-density phase of the specimens dominated during the four cycles of impact, and the compression-density process absorbed a large amount of impact energy and did not cause positive damage to the specimens.

(4) Under triaxial pressure conditions, the coal body had a significant strain rate effect. The higher the impact velocity, the higher the peak stress that the specimen can reach, and the corresponding peak strain rate is also higher.

(5) Under the triaxial pressure conditions, the coal body is broken to different degrees at different impact velocities. The higher the impact velocity, the greater the energy generated by the incident wave, and the average incident energy is 178.8 J, 229.2 J, 271.8 J and 325.4 J in order, the more serious the damage or fragmentation of the specimen is, and the more energy consumed by the fragmentation. At lower impact velocity, the specimen does not appear separated crushing; with the increase of impact velocity, the specimen begins to break into large pieces; at higher impact velocity, the specimen will break into small pieces and produce a large amount of debris. Combined with the engineering practice, the mining and crushing efficiency of coal and rock can be improved by increasing the impact velocity.

---

## 6.2 Outlooks

Due to the limitations of experimental conditions and personal expertise, there are still shortcomings in this study, and some directions still need further research to explore.

(1) The specimen chosen for the experiment is a single coal body, and the cyclic impact load experiment can be considered next for the combined coal rock specimen to analyze the damage evolution effect of the combined coal rock.

(2) The dynamic damage strength of coal rocks has a certain pattern with the length-to-diameter ratio of the specimen, and the next consideration is to conduct cyclic impact load experiments on coal rocks with different length-to-diameter ratios to analyze the effect of the length-to-diameter ratio on the dynamic damage strength of the specimen.

(3) The presence of gas in the actual coal seam will also affect the dynamic mechanical properties of the coal, so we can conduct cyclic impact load experiments on the coal containing gas to analyze the damage evolution law and the dynamic load damage law of the coal containing gas.

## Reference

---

- [1] Xie Heping. Research concept and expected results of "deep rock mechanics and mining theory"[J]. *Engineering Science and Technology*,2017,49(02):1-16.
- [2] Xie Heping,Gao Feng,Ju Yang. Research and exploration on the mechanics of deep rock masses[J]. *Journal of Rock Mechanics and Engineering*,2015,34(11):2161-2178.
- [3] Li Xibing,Zhou Jian,Wang Shaofeng,Liu Bing. Review and exploration of deep solid resources mining[J]. *Chinese Journal of Nonferrous Metals*,2017,27(06):1236-1262.
- [4] Xie Heping, Peng Su Ping, He Manchao. Basic theory and engineering practice of deep mining [M]. Beijing:Science Press,2005:1-35.
- [5] Zhao Shengcai. Resource extraction and subsurface engineering under deep high stresses - A review of the 175th Xiangshan Conference[J]. *Advances in Earth Sciences*, 2002, (02): 295-298.
- [6] Liu Huanxin,Wang Jianbo,Zhao Jie,et al. A preliminary investigation of key technical problems and solutions for deep well mining[J]. *Mining Research and Development*, 2018, 38(05): 1-5.
- [7] QI Qingxin, PAN Yishan, LI Haitao, JIANG Deyi, SHU Longyong, ZHAO Shankun, ZHANG Yongzhong, PAN Junfeng, LI Hongyan, PAN Pengzhi. Theoretical basis and key technology of coal rock power disaster prevention and control in deep mining coal mines[J]. *Journal of Coal*,2020,45(05):1567-1584.
- [8] He Jiang, Dou Linming, Cao Jinrong, Wu Jianghu, Cao Lihua. Mechanism of impact mine pressure in horizontal sectionalized integrated mining of sharply inclined extra-thick coal seams[J]. *Journal of Coal*,2020,45(05):1701-1709.
- [9] Zhai M.H., Jiang F.X., Qi Q.X., Guo X.S., Liu Y., Zhu S.T. Research and application of classification and prevention system for impact ground pressure[J]. *Journal of Coal*,2017,42(12):3116-3124.
- [10]Zhao Pengxiang, Zhuo Risheng, Li Shugang, Shu Chi-Min, Laiwang Bin, Jia Yongyong, Shi Yu, Suo Liang. Analysis of advancing speed effect in gas safety extraction channels and pressure-relief gas extraction[J]. *Fuel*, 2020, 265(4): 116825.
- [11]Liu Shuxin,Lu Sizuo,Chen Yang. Study of rockburst propensity in a deep mine area based on multiple criteria[J]. *Mining Research and Development*, 2017, 37(02): 9-12.

- [12]He F, Xu YN, Qiao GANG, et al. Distribution characteristics of geological hazards in Chinese mines[J]. Geological Bulletin, 2012, (31): 476-485.
- [13]Liu ZQ, Ma HSS, Mou YJ. Stability analysis and management measures of the collapsed critical rock body at the exit of Gulgou Tunnel[J]. Roadbed Engineering, 2020, (02): 216-221.
- [14]Zhang Zanguo, Ma Zhiyong, Wang Zhen. Research on gas prevention and control technology system of impact ground pressure coal seam[J]. Mining Safety and Environmental Protection, 2019, 46(06): 66-71.
- [15]WANG Enyuan, FENG Junjun, ZHANG Qiming, KONG Xiangguo, LIU Xiaofei. Mechanism of impact ground pressure stress wave action[J]. Journal of Coal, 2020, 45(01): 100-110.
- [16]Hoek E, Brown ET. Empirical strength criterion for rock masses[J]. Journal of the Geotechnical Engineering Division, 1982, 106(15715): 1013-1035.
- [17]Jiang Yaodong, Pan Yishan, Jiang Fuxing, Dou Linming, Ju Yang. Mechanism and prevention of impact ground pressure in coal mining in China[J]. Journal of Coal, 2014, 39(02): 205-213.
- [18]Huang Lixing, Chen Yibai. Status and development of rock dynamics research in China[J]. Journal of Rock Mechanics and Engineering, 2003(11): 1881-1886.
- [19]Huang Lixing. Achievements and trends in rock dynamics research[J]. Geotechnics, 2011, 32(10): 2889-2900.
- [20]K W Hillier, H Kolsky. An Investigation of the Dynamic Elastic Properties of Some High Polymers[J]. 1949, 62(2): 111-121.
- [21]Xia Kaiwen, Wang Shuai, Xu Ying, Chen Rong, Wu Gangbiao. Advances in experimental research on deep rock dynamics[J]. Journal of Rock Mechanics and Engineering, 2021, 40(03): 448-475.
- [22]Wang Shuhong, Zhang Xiaode, Chen Meng, Wang Feiasa, Cai Yunsheng. Application of SHPB system in experimental teaching of rock mechanics and exploration of curriculum reform[J]. Experimental Technology and Management, 2020, 37(02): 182-185.
- [23]ZHANG Jiafan, GAO Zhuang, CHENG Shufan, ZHANG Huimei. Experimental study on the dynamic characteristics of coal rock under impact loading[J]. Coal Mine Safety, 2020, 51(08): 23-27.
- [24]Liu Buxian, Huang Jinglin, Wang Zeyun, Liu Li. Study on damage evolution and acoustic emission characteristics of uniaxially compressed coal rocks[J]. Journal of Rock Mechanics and Engineering, 2009, 28(S1): 3234-3238.

- [25]Liu Xiaohui,Zhang Ru,Liu Jianfeng. Experimental study of coal rock impact dynamics under different strain rates[J]. Journal of Coal,2012,37(09):1528-1534.
- [26]Lv Xiaocong,Xu Jinyu,Zhang Long,Zhang Lei. Impact dynamics test of large diameter SHPB system hornblende[J]. Journal of Military Engineering,2010,31(S1):227-233.
- [27]YANG Yongjie,SONG Yang,CHEN Shaojie. Experimental study of strength and deformation characteristics of triaxially compressed coal rocks[J]. Journal of Coal,2006(02):150-153.
- [28][28] Liang W.M., Liu H., Li M.M., Yue G.W.. Study of uniaxial/triaxial impact dynamics performance of structurally anisotropic coal bodies[J/OL]. Journal of Process Engineering:1-9[2021-04-06].
- [29]Zuber, M.d., Sawyer, W.K., Schraufnagel, R.A., et al. The Use of Simulation and History Matching to Determine Critical Coalbed Methane Reservoir Properties[C]. Low Permeability Reservoirs Symposium, US, Denver, 1987:307-316.
- [30]Zhai Y , Guowei M A , Zhao J , et al. COMPARISON OF DYNAMIC CAPABILITIES OF GRANITE AND CONCRETE UNDER UNIAXIAL IMPACT COMPRESSIVE LOADING[J]. Chinese Journal of Rock Mechanics and Engineering, 2007, 26(4):762-768.
- [31]FREW D J, FORRESTAL M J, CHEN W. A split Hopkinson pressure bar technique to determine compressive stress-strain data for rock materials[J]. Experimental Mechanics, 2001, 41(1) : 40 - 46.
- [32]Ju Yang, Wang Huijie, Yang Yongming, et al.Numerical simulation of mechanisms of deformation failure and disipation in porous rock media subjected to wave stresses[J].Science in China, Series E:Technological Sciences, 2010, 53(4):1098-1113.
- [33]Li Xibing, Zhou Zilong, Ye Zhouyuan, Ma Chunde, Zhao Fujun, Zuo Yujun, Hong Liang. Study on the mechanical properties of rock with combined dynamic and static loading[J]. Journal of Rock Mechanics and Engineering,2008(07):1387-1395.
- [34]Guo Deyong,Lv Pengfei,Zhao Jiechao,Zhu Tongkong. Impact deformation damage characteristics of coal rock and its intrinsic model[J]. Journal of Coal,2018,43(08):2233-2242.
- [35]ZHANG Ying,LI Ming,WANG Kehui,CHU Zhe. Experimental study on dynamic mechanical properties of rocks[J]. Journal of Rock Mechanics and Engineering,2010,29(S2):4153-4158.

- [36]Zhang Pengpeng,Gong Nengping,Zhou Jian. Numerical simulation of SHPB active enclosure pressure experiments on coal rock materials[J]. Coal Technology,2018,37(05):76-78.
- [37]Li Chengwu, Xie Beijing, Yang Wei, et al. Characterization of near transient magnetic field changes during coal impact damage[J]. Journal of Rock Mechanics and Engineering, 2012, 31(05): 973-981.
- [38]Li Chengwu, Wang Jingui, Xie Beijing, et al. Experimental numerical simulation of coal rock SHPB based on HJC intrinsic structure model[J]. Journal of Mining and Safety Engineering, 2016, 33(01): 158-164.
- [39]Li Chengwu,Wang Jingui,Hu Po,Wang Chuan. Numerical simulation study on the experimental passive surrounding pressure of coal rock material SHPB[J]. Journal of Mining and Safety Engineering,2014,31(06):957-962.
- [40]WANG Bin, LI Xibing, YIN Tubing, MA Chunde, YIN Zhiqiang, LI Zhiguo. Experimental study on the dynamic strength of water-saturated sandstone by SHPB[J]. Journal of Rock Mechanics and Engineering,2010,29(05):1003-1009.
- [41]Zhang Yaqi, Zhou Zonghong, Jin Xiaochuan, et al. Study on the damage characteristics of dolomite debris under combined dynamic and static loading [J]. Mining Research and Development, 2014, 34( 7) : 54 - 58.
- [42]L.Y. Li, C.Q. Xu, H.H. Xie, Y.J. Ju, X. Ma, Z.C. Han. Experimental study of rock damage energy law under different impact velocities[J]. Journal of Coal,2011,36(12):2007-2011.
- [43]Liu Junzhong, Xu Jinyu, Lv Xiaocong, et al. Experimental study of dynamic mechanical properties of hornblende under impact compression loading[J]. Journal of Rock Mechanics and Engineering, 2009, 28( 10) : 2113 - 2120.
- [44]Deng Jian, Bian Li.Response and energy disipation of rock under stochastic stres waves[J].Journal of Central South University of Technology(English Edition), 2007, 14(1):111-114.
- [45]Xie, Beijing, Zhao, Zeming, Xu, Xiaomeng, et al. Ontogenetic model and numerical simulation of HJC for hammer damage of gas-bearing coal[J]. Journal of Coal, 2018, 43(10): 2789-2799.
- [46]Xie B, Yan Z, Du Y, et al. Determination of Holmquist-Johnson-Cook Constitutive Parameters of Coal: Laboratory Study and Numerical Simulation[J]. Processes, 2019, 7(6): 386.
- [47]Xie, Beijing. Experimental study on the kinetic characteristics of coal impact damage and magnetic field variation characteristics [D]. China University of Mining and Technology (Beijing),2013.



- [48] Liu Baochen, Zhang Jiasheng, Du Qizhong, et al. Size effect of compressive strength of rocks[J]. Journal of Rock Mechanics and Engineering, 1998, 17(6): 611-614.
- [49] Yang Shengqi, Su Chengdong, Ming Pingmei, et al. Study on the method and mechanism of rock strength size effect[J]. Journal of Jiaozuo Institute of Technology: Natural Science Edition, 2002, (5): 323-325.
- [50] YANG Shengqi, SU Chengdong, XU Weiya. Experimental and theoretical studies on the size effect of rock materials[J]. Engineering Mechanics, 2005, 22(4): 112-118.
- [51] Li F, Fang Shuhao, Bi Mingxin, Tian Jing. Numerical simulation of dynamic damage of coal rock mass under dynamic loading[J]. Coal Technology, 2017, 36(11): 167-169.
- [52] Wang Dengke, Liu Shumin, Wei Jianping, Wang Honglei, Peng Ming. Intensity-based statistical damage intrinsic model and analysis of coal under impact damage conditions[J]. Journal of Coal, 2016, 41(12): 3024-3031.
- [53] Wang R.P., Sun T.M.. Study on dynamic damage time during coal impact damage[J]. Energy Technology and Management, 2013, 38(03): 37-39.
- [54] SONG Honghua, ZHAO Yi-Xin, JIANG Yaodong, ZHANG Xiu-Ze. Influence of non-homogeneity of coal rock on its damage characteristics under uniaxial compression conditions[J]. Journal of Coal, 2017, 42(12): 3125-3132.
- [55] Li Xibing, Gu Desheng. Rational loading waveforms in dynamic stress-strain allogram testing of rocks under impact loading[J]. Explosion and Impact, 1993, 13(2): 125-131.
- [56] Li Xibing, Zhou Zilong, Wang Weihua. Construction of ideal punches for SHPB devices using finite elements and neural networks[J]. Journal of Rock Mechanics and Engineering, 2005, 24(23): 4 215-4 219.
- [57] LI X B, LOK T SZHAO J. Dynamic characteristics of granite subjected to intermediate loading rate[J]. Rock Mechanics and Rock Engineering, 2005, 38(1): 21-39.
- [58] Zhu Jingjing, Li Xibing, Gong Fengqiang, Wang Shiming. Dynamics of rock under uniaxial cyclic impact and its damage model[J]. Journal of Geotechnical Engineering, 2013, 35(03): 531-539.
- [59] WANG Zhiliang, YANG Hui, TIAN Nuocheng. Mechanical properties and damage evolution mechanism of granite under uniaxial cyclic impact[J]. Journal of Harbin Institute of Technology, 2020, 52(02): 59-66.

- [60] SONG Xiaolong, GAO Wenhua, JI Jinming, YE Mingban, ZHANG Dengjie. Influence of blasting vibration on the evolutionary effect of damage in tunnel surrounding rock[J]. *Vibration and shock*,2020,39(24):54-62.
- [61] Jin Peijian, Wang Enyuan, Song Dazhao, Huang Ning, Wang Jiheng. Experimental study on the law of electromagnetic radiation of coal rock by uniaxial cyclic loading[J]. *Coal Mine Safety*,2013,44(05):46-48.
- [62] Liu YJ, Chen P, Zhang LQ, Li SY. Experimental study on cyclic loading damage surface potential of coal containing gas [J]. *Industrial and mining automation*,2015,41(09):26-30.
- [63] Liu Shao-He,Xu Jin-Yu,Wang Peng,Zhang Guo-Xi. Mechanical and ultrasonic analysis of cyclic impact damage in sandstone under circumferential pressure conditions[J]. *Vibration and Impact*,2015,34(01):190-194.
- [64] Yu Yang,Xu Qian,Diao Xinhong,Yan Zhiyu. Influence of cyclic impact on the characteristics of sandstone under the action of circumferential pressure[J]. *Journal of Huazhong University of Science and Technology (Natural Science Edition)*,2019,47(06):127-132.
- [65] Dai B, Luo XY, Shan QW, Chen Y, Liu Y. Analysis of damage characteristics and energy dissipation of rock containing holes under cyclic impact loading[J]. *Chinese Journal of Safety Science*,2020,30(07):69-77.
- [66] Lin, D.N., Chen, Shouru. Experimental study on the damage law of rocks under cyclic impact loading[J]. *Journal of Rock Mechanics and Engineering*,2005(22):4094-4098.
- [67] Lin DANENG, Chen SHOURU, Liu YUPING. Experimental study on the evolution of peritectic effects of cyclic impact damage in rocks[J]. *Mining and Metallurgical Engineering*,2005(04):12-15.
- [68] Xu Qian. Analysis of structural and mechanical properties of sandstone under cyclic impact loading[D]. East China Jiaotong University,2019.
- [69] Jin Jiefang,Li Xibing,Chang Junran,Tao Wei,Qiu Can. Stress-strain curves and stress-wave properties of rocks under cyclic impact[J]. *Explosion and Impact*,2013,33(06):613-619.
- [70] Li N, Wang EY, Zhao ENL, Ma YK, Xu FL, Qian WH. Experimental study on acoustic emission of damage damage by cyclic loading and graded loading of rocks[J]. *Journal of Coal*,2010,35(07):1099-1103.
- [71] Yu Xianbin, Xie Qiang, Li Xinyi, Nayukang, Song Zhanping. Cyclic loading experiments on direct tensile and compressive deformation of rocks with a two-

- modulus principal structure model[J]. Journal of Geotechnical Engineering,2005(09):988-993.
- [72] He Manchao. The conceptual system and engineering evaluation index of the deep part[J]. Journal of Rock Mechanics and Engineering,2005(16):2854-2858.
- [73] Zhou Hongwei, Xie Heping, Zuo Jianping. Progress in the study of mechanical behavior of rocks under deep high ground stress[J]. Advances in Mechanics,2005(01):91-99.
- [74] Xie Heping,Zhou Hongwei,Xue Dongjie,Wang Hongwei,Zhang Ru,Gao Feng. Research and reflection on deep coal mining and ultimate mining depth[J]. Journal of Coal,2012,37(04):535-542.
- [75] Yuan Liang. Consideration of deep coal and gas co-mining strategy in China[J]. Journal of Coal,2016,41(01):1-6.
- [76] Li H. M., Fu K. Main technical problems and countermeasures faced by deep mining in coal mines[J]. Journal of Mining and Safety Engineering, 2006(04):468-471.
- [77] Peng, Su-Ping. Research status and future development trend of deep coal resources and geological evaluation[J]. Coal,2008(02):1-11+27.
- [78] Sun J, Wang S J. Rock mechanics and rock engineering in China: developments and current state-of-the-art [J]. International Journal of Rock Mechanics and Mining Science, 2000(37):447-465.
- [79] Lu, F.Y.. Hopkinson rod experimental techniques [M]. Science Press. 2013:23-44.
- [80] Renliang Shan, Yusheng Jiang, Baoqiang Li. Obtaining dynamic complete stress-strain curves for rock using the Split Hopkinson Pressure Bar technique[J]. International Journal of Rock Mechanics and Mining Sciences, 2000, 37:983~992.
- [81] Hong, Liang. Study on the dimensional effect of rock strength and crushing energy characteristics under impact loading [D]. Changsha: Central South University, 2008:55-80.
- [82] Du Jing. Study of rock impact dynamics characteristics under different length-to-diameter ratios [D]. Changsha: Central South University, 2011.
- [83] Gao Guangfa, Li Yongchi, Liu Weiguo. Experimental techniques for SHPB of porous hard and brittle materials[J]. Mechanics and Practice, 2011, 33(06):35-39.
- [84] Xueying Zhang, Huai-Ning Ruan, Rainbow Jia. Progress of rock damage mechanics theory[J]. Sichuan Construction Science Research, 2010, 36(02):134-138.

- [85]Wu G,Sun Jun,Wu C-R. Damage mechanics analysis of unloading damage of intact rock masses under complex stress state[J]. Journal of River Sea University,1997(03):46-51.
- [86]Cao WG, Zhao MH, Tang XJ. Statistical damage simulation of rock fracture process[J]. Journal of Geotechnical Engineering,2003(02):184-187.
- [87]Li Shuchun,Xu Jiang,Li Kegang. A statistical intrinsic model of rock damage based on the correction of initial damage coefficient[J]. Journal of Sichuan University (Engineering Science Edition), 2007(06):41-44.
- [88]Feng Xibiao, Yu Shouwen. Fine-scale damage mechanics of quasi-brittle materials [M]. Beijing: Higher Education Press, 2003.
- [89]Xie Heping, Ju Yang, Li Li Yun. Rock strength and integral damage criterion based on the principle of energy dissipation and release [J]. Journal of Rock Mechanics and Engineering,2005(17):3003-3010.
- [90]Yang Qingshe, Zhang Changqing. Rock damage and detection [M]. Shaanxi: Shaanxi Science and Technology Press, 1998.
- [91]Jin Jiefang,Li Xibing,Yin Zhiqiang,Du Kun. Effect of axial pressure and number of cyclic impacts on dynamic mechanical properties of sandstone[J]. Journal of Coal,2012,37(06):923-930.
- [92]WANG Jianguo,LIANG Shufeng,GAO Quanchen,LI Xianglong,WANG Lina,ZHAO Yan. Experimental study on the effect of nodal dip angle on impact energy transfer of rock-like [J]. Journal of Central South University (Natural Science Edition),2018,49(05):1237-1243.
- [93]JU Yang,LI Yexue,XIE Heping,SONG Zhenduo,TIAN Lu Lu. Stress fluctuations and energy dissipation in jointed rocks[J]. Journal of Rock Mechanics and Engineering,2006(12):2426-2434.
- [94]Li Yexue, Liu Jianfeng, Qin Li. Experimental study on rule of energy dissipation of stress wave across rock joint[J]. Journal of Experimental Mechanics, 2011, 26(1): 85–90.



中国矿业大学(北京)  
CHINA UNIVERSITY OF MINING & TECHNOLOGY-BEIJING

## Thesis Grade

Thesis topic: Experimental study on dynamic failure characteristics  
of confined coal under cyclic impact load

Author : Chunyang Dong

Supervisor: Beijing Xie Grade : 94 Signature : Beijing Xie  
Co-Supervisor: \_\_\_\_\_ Grade : \_\_\_\_\_ Signature : \_\_\_\_\_